Measurement report: Formation and brownness of aqueous secondary organic aerosol from the aged biomass-burning emissions in the Sichuan Basin, China

Chao Peng[1,2,3,4], Yan Ding[4], Zhenliang Li[1,2,3], Tianyu Zhai[4], Xinping Yang[4], Mi Tian[6], Yang Chen[5], Xin Long[5], Haohui Tang[6], Guangming Shi[7], Liuyi Zhang[8], Kangyin Zhang[8], Fumo Yang[7], and Chongzhi Zhai[1,2,3]

[1]Chongqing Academy of Ecology and Environmental Sciences, Chongqing, 401336, China

[2]Chongqing Branch Academy of Chinese Research Academy of Environmental Sciences, Chongqing, 401336, China

[3]Chongqing Key Laboratory of Urban Atmospheric Environment Observation and Pollution Prevention, Chongqing, 401336, China

[4]Chinese Research Academy of Environmental Sciences, Beijing 100012, China

[5]Chongqing Institute of Green and Intelligent Technology, Chinese Academy of Sciences, Chongqing, 400714, China

[6]College of Environment and Ecology, Chongqing University, Chongqing, 400045, China

[7]College of Carbon Neutrality Future Technology, Sichuan University, Chengdu, 610065, China

[8]Chongqing Three Gorges University, Wanzhou, 404000, China

Correspondence: Chao Peng (pengchao0623@sina.com) and Chongzhi Zhai (czz66818@sina.com)

Abstract. Secondary organic aerosol (SOA) formed via complex chemical mechanisms was the major contributor to atmospheric aerosol pollution and climate forcing worldwide. The aqueous-phase oxidation was an important pathway for SOA formation and the aqueous SOA (aqSOA) exhibited absorption properties across ultraviolet to visible range. Here, we reported the formation and absorption properties of aqSOA in the Sichuan Basin, China. aqSOA was originated from the aged biomass-burning emissions via aqueous-phase reactions instead of photo-chemical reactions under high aerosol liquid water content (ALWC) conditions, especially during the polluted period. The substantial impact on brown carbon (BrC) absorption from SOA was observed from 370 nm to 660 nm (27.5%−43.2%). This study highlighted the significant contribution of aqSOA formation from aged biomass-burning emissions to the BrC budget and absorption, especially at night. The mean aerosol absorption Ångström exponents from 370 nm to 880 nm ($AAE_{370-880}$) was 1.95, higher than that observed in fresh and photo-chemically aged biomass-burning emissions. This study revealed the aqSOA formation and brownness from aged biomass-burning emissions and highlighted the importance of aqueous-phase reactions on aerosol pollution and absorption.

Keywords: Particulate matter; Secondary organic aerosol; Aqueous-phase oxidation; Aged biomass-burning emissions; Brown carbon.

1 Introduction

Organic aerosol (OA) is the dominant component (20 to 90%) of atmospheric aerosol with significantly implications for air quality and climate forcing (Jimenez et al., 2009). Numerous field observations indicated that secondary OA (SOA), formed by atmospheric oxidation of volatile organic compounds (VOCs) and primary OA (POA), accounted for most of OA worldwide (Ervens et al., 2011; Huang et al., 2014; Kourtchev et al., 2016). Recent results showed that aqueous-phase oxidation is an important pathway for SOA formation and these SOA production (aqSOA) exhibit absorption properties across ultraviolet (UV) to visible (Vis) range (Gilardoni et al., 2016; Lim et al., 2010; McNeill 2015; Powelson et al., 2014; Sun et al., 2010). However, the formation mechanisms and absorption properties of aqSOA are poorly understood, hindering to improvement of air quality and reducing the uncertainties in global climate estimations.

An increasing number of studies pointed toward aqSOA as a major SOA could form in fogs, clouds, and aerosol water (Ervens et al., 2011; Ortiz-Montalvo et al., 2012; Tan et al., 2012; Xu et al., 2022). And the oxygenated VOCs (OVOCs) with large water-soluble and low Henry's constant (i.e., methylglyoxal and glycolaldehyde) are the important aqSOA precursors (Ortiz-Montalvo et al., 2012; Tan et al., 2012). A few laboratory studies investigated the levoglucosan and phenolic species produced from biomass burning could also act as aqSOA precursors (Yu et al., 2016; Zhao et al., 2014). Gilardoni et al. (2016) reported direct ambient observations of aqSOA formation from biomass-burning emissions in fog water and wet aerosol. Additionally,

recent studies indicated that aqSOA with high molecular weight (i.e., 4-ethylphenol) formed by aqueous-phase photochemical oxidation showed strong light absorptivity within UV range (Herrmann et al., 2015; Ye et al., 2019). Previous laboratory studies also demonstrated that aqSOA, such as π-conjugated compounds and imidazole with C=N bonds produced by aldol condensation and aqueous-phase carbonyl compound reactions respectively, would strongly absorb light at near-UV (Drozd and McNeill, 2014; Kampf et al., 2012; Nozière and Esteve, 2007; Powelson et al., 2014). Despite numerous studies reported on the formation and optical properties of aqSOA, limited research on its ambient observations hinder to better understand the role of aqSOA in atmospheric chemistry and climate.

China experienced severe $PM_{2.5}$ pollution under the stagnant high-humidity conditions, when SOA as the major component was originated from fossil fuel combustion and biomass burning (Huang et al., 2014; Wang et al., 2016; Wang et al., 2021; Xu et al., 2022). Field observations indicated that highly oxidized SOA could form through aqueous-phase processing driven by acid-catalyzed oxidation (Meng et al., 2020; Xu et al., 2017), and aqSOA is formed from biomass-burning OA (BBOA) and fossil-fuel OA via aqueous-phase reactions (Wang et al., 2021; Zhao et al., 2019). A few laboratory studies found aqueous-phase reactions were an important oxidation pathway for nitrophenol products (i.e., 5-nitrovanillin and 4-nitroguaiacol) with strong UV absorption and higher formation and transformation rates were observed in more acidic solutions (Kroflic et al., 2015; Li et al., 2023; Pang et al., 2019; Yang et al., 2021). However, observations on aqSOA formation and optical properties in China

are limited and most research concentrate on the North China Plain (NCP). Similar to NCP, the Sichuan Basin (SCB) characterized by high humidity and frequent biomass burning is also the main region with severe aerosol pollution in China (Tian et al., 2019; Wang et al., 2018; Yang et al., 2011). Previous research indicated that aqSOA from different regions exhibited distinct formation mechanisms and optical properties, due to the diverse sources and ambient conditions (Bao et al., 2023; Bao et al., 2024; Wang et al., 2021; Xu et al., 2017). For instance, Wang et al. (2021) revealed fast aqueous-phase conversion of fossil-fuel primary organic aerosol (FF-POA) to aqSOA under high-humidity conditions during a Beijing winter haze event, and found that aqSOA exhibited much lower light absorption than its primary precursor due to decreased aromaticity. Similarly, Huang et al. (2023) illustrated that the aqueous-phase oxidation of fossil fuel combustion emissions played a critical role in SOA formation under high RH conditions. Unlike these studies in NCP, the effect of aqueous-phase reactions on oxygenated OA (OOA) formation was significant when aerosol liquid water content (ALWC) was below 200 μg m^{-3}, but was insignificant when ALWC > 200 μg m^{-3} in SCB. Additionally, the aqueous-phase oxidation process probably did not play a role in the decay of BrC during summer in Chengdu (Bao et al., 2024). Currently, few studies explored the dynamic evolution and optical properties of aqSOA, and the knowledge of ambient aqSOA processing is still limited in SCB. Therefore, a more detailed characterization of aqSOA formation and optical properties is of great importance to reveal the key factors contributing to haze formation.

Here a time-of-flight aerosol chemical speciation monitor (ToF-ACSM) and a series of collocated instruments were used to characterize aqSOA dynamic evolution from biomass burning under real ambient conditions in a typical city with relatively serious air pollution in SCB from October 21 to November 23, 2022. We observed that the haze formation was largely driven by BBOA and aqSOA. We demonstrated aqSOA was originated from the aged BBOA via aqueous-phase reactions. Finally, we further showed that aqSOA produced from aged BBOA were strong UV absorption with positive radiative forcing. These results revealed the aqSOA formation and brownness from aged biomass-burning emissions and helped simulate the associated influences on atmospheric chemistry and climate.

2 Methods

2.1 Sampling site

An intensive field campaign on the chemical and physical properties of aerosol was conducted at a measurement site in a city affected by severe aerosol pollution (Yongchuan, 29°21′25″ N, 105°54′6″ E) from October 21 to November 23, 2022. This is a typical urban site surrounded by restaurants, shopping malls, and residential buildings, and the site is located in a parallel ridge-and-valley area between two megacities in SCB (Chongqing center and Chengdu) (Fig. S1). It was primarily influenced by multiple local emissions from traffic (arterial roads to the east 600 m and west 300 m) and a variety of residential sources (i.e., biomass burning and fossil fuel combustion). There was no interference of dynamics from neighboring buildings,

and measurements at the site helped understand the characteristics of haze pollution dynamic evolution.

2.2 Instrumentation

During the campaign, the non-refractory aerosol (NR-$PM_{2.5}$) species, including OA, ammonium (NH_4), nitrates (NO_3), sulfates (SO_4), and chlorides (Chl), were measured on-line by ToF-ACSM (Aerodyne Research Inc.). Ambient aerosols were pumped into ToF-ACSM at a flow rate of 3 L min^{-1} through a $PM_{2.5}$ cyclone (URG-2000-30ED) and a Nafion dryer (MD-110-48S, Perma Pure, Inc.) reducing the relative humidity to below 30%. The measurement principle was described in detail in the previous studies (Fröhlich et al., 2013; Ng et al., 2011c).

A seven-wavelength Aethalometer (AE33, Magee Scientific) was used to measure the aerosol light absorption (Abs_λ) and equivalent black carbon (BC_λ) mass concentrations in real time at 370, 470, 520, 590, 660, 880, and 950 nm. The sampled particles were dried by a Nafion dryer (MD-70024S-3, Perma Pure, Inc.) before entering into AE33. The light attenuation coefficients were converted to Abs_λ based on the real-time compensation parameter, and the nonlinear loading effects of quartz filters were dealt with on-line by the parallel measurements of attenuation values (ATN1 and ATN2) (Coen et al., 2010; Drinovec et al., 2015). The scattering effects of quartz filters were modified automatically by a fixed multiple scattering parameter (2.14). Detailed measurement methods and principles of AE33 can be found in Drinovec et al. (2015).

During the campaign, the gaseous species (including O_3, NO_2, and CO) were continuously measured by gas analyzers (49i, 42i, and 48i, Thermo Scientific), that were maintained and calibrated weekly. Hourly meteorological parameters data including temperature (T), relative humidity (RH) and $PM_{2.5}$ mass concentrations were obtained on-line from the measurements at the National Environmental Monitoring Station, which was close to our sampling site (http://www.cnemc.cn/).

2.3 Data analysis

2.3.1 ToF-ACSM data analysis

The raw mass spectra data measured by ToF-ACSM were analyzed using Tofware v2.5.13 (Tofwerk AG) in Igor Pro 6.37 (WaveMetrics, Inc.). The ionization efficiency (IE) and relative ionization efficiency (RIEs) were regularly calibrated using a scanning mobility particle sizer with a differential mobility analyzer (SMPS 3081A, TSI) and a condensation particle counter (CPC 3775, TSI). The comprehensive overview of the operation and calibration procedures of ToF-ACSM can be found in Bao et al. (2023). In accordance with previous studies, the default RIEs values for OA, NO_3, and Chl were set to 1.4, 1.1, and 1.3, respectively (Canagaratna et al., 2007; Elser et al., 2016). The IE value (236 ions pg^{-1}) and RIEs of SO_4 (1.2) and NH_4 (4.3) were estimated from the calibrations of pure ammonium nitrate and ammonium sulfate, respectively. Meanwhile, a particle collection efficiency (CE) was introduced to compensate for the particle loss, as the acidity, the contribution of ammonium nitrate (ANMF) and phase state changed the particle

bounce effects at the vaporiser (Matthew et al., 2008). Middlebrook et al. (2012) developed a CE algorithm for ToF-ACSM to quantify the aerosol species. Their results indicated that a constant CE value of 0.45 should be used when: (1) the ANMF is below 40%, or (2) particles are partially or fully neutralized. In this study, aerosol particles were dried by Nafion dryer (RH < 30%) before sampling by ToF-ACSM, and the ANMF was always below 40%. As shown in Fig. S2, the average ratio of the measured NH_4 to the predicted NH_4 needed to fully neutralize the SO_4, NO_3 and Chl was approximately 1. All of these conditions did not affect the CE value that had usually been used at this site. The typical default CE value (0.5) was applied during the whole sampling period, which was consistent with previous research (Bao et al., 2025; Peng et al., 2025; Sun et al., 2016a; Sun et al., 2016b; Zhao et al., 2019). While the typical default CE is 10% higher than 0.45, the difference is small considering the 30% uncertainty determined for CE (Bahreini et al., 2009). Additionally, the strong correlation between NR-$PM_{2.5}$ and $PM_{2.5}$ mass concentrations supported that the CE value was reasonable (Fig. S3).

The mass spectral matrix of OA for m/z 10−120 was analyzed by positive matrix factorization (PMF) and multilinear engine (ME2) implemented with the SoFi (Source Finder) (version 6.3, Canonaco et al., 2013; Paatero 1999; Paatero and Tapper 1994). Briefly, unconstrained PMF was used to determine the numbers and types of source factors, then the restriction method ME2 was used to minimize PMF rotational ambiguity by the *a*-values from 0 to 1 with a step of 0.1 (Elser et al., 2016; Wang et al., 2019; Zhong et al., 2021). The ions data with signal-to-noise (S/N) lower than 0.2

were discarded, and those S/N from 0.2−2 were downweighted by a factor of 2 (Bao et al., 2023; Paatero and Hopke 2003). Finally, five OA factors with function of the rotational parameter (f_{peak} = 0) were identified, including three POA factors (i.e., BBOA, coal-combustion OA (CCOA), and hydrocarbon-like OA (HOA)) and two SOA factors (i.e., OOA and aqSOA) (Fig. S9 and S10). We present detailed diagnostic plots of the PMF results in the supporting information (Fig. S4−S10). The details of OA source apportionment procedures are described in SI Text S1.

2.3.2 Aerosol liquid water content

The ALWC is controlled by meteorological conditions (T and RH) and also by inorganic and organic components. During the campaign, the ALWC with inorganic species was estimated by the ISORROPIA-II model based on the ammonium, nitrates, sulfates, and chlorides mass concentrations from ToF-ACSM and the meteorological parameters (T and RH) from National Environmental Monitoring Station (Fountoukis and Nenes, 2007). Here, the forward type and metastable mode were used in the ISORROPIA-II model (Hennigan et al., 2015). The thermodynamic equilibrium of the NH_4^+−SO_4^{2-}−NO_3^-−Cl^-−H_2O system was modeled and ALWC was then calculated. Consistent with previous research, the organic contribution for ALWC was calculated by Zdanovskii−Stokes−Robinson (ZSR) mixing rule as discussed in SI Text S2 (Guo et al., 2015; Huang et al., 2020; Nguyen et al., 2016; Xu et al., 2022). In this study, the ALWC with organic species ranged from 0.1 to 35.2 μg m^{-3}, with an average of 1.9 ± 3.0 μg m^{-3}, taking up 3.7 ± 2.2% of total ALWC. As organic species had minor effects

on total ALWC (< 5%), the ALWC was determined only considering inorganic species (Chen et al., 2021; Guo et al., 2015; Liu et al., 2017).

2.3.3 Light absorption measurements

The Abs_{λ} was divided into BC and brown carbon (BrC, a group of colored OA compounds) absorption ($Abs_{\lambda,BC}$ and $Abs_{\lambda,BrC}$) ($Abs_{\lambda}=Abs_{\lambda,BC}+Abs_{\lambda,BrC}$) and characterized by the absorption Ångström exponents (AAE) (Laskin et al., 2015). Here, Abs_{λ} was determined dependent BC_{λ} mass concentrations ($Abs_{\lambda}=BC_{\lambda}\times MAC_{\lambda}$). We assumed the mass absorption cross-section of aerosols (MAC_{λ}) were 18.47, 14.54, 13.14, 11.58, 10.35, 7.77, and 7.19 $m^2\ g^{-1}$ at 370, 470, 520, 590, 660, 880, and 950 nm, respectively (Drinovec et al., 2015; Zhu et al., 2017). Here, we assumed that Abs_{880} was sole from BC, then the following formula was used to determine $Abs_{\lambda,BC}$ values: $Abs_{\lambda,BC}=Abs_{880}\times(880/\lambda)^{-AAE_{BC}}$ (Drinovec et al., 2015; Kirchstetter and Novakov, 2004; Moosmüller et al., 2009; Qin et al., 2018; Zhu et al., 2017). The AAE of BC (AAE_{BC}) value was obtained from the equality: $AAE_{BC}=-\log(Abs_{880}/Abs_{950})\div\log(880/950)$ (Wang et al., 2021). A detailed description of $Abs_{\lambda,BC}$ and $Abs_{\lambda,BrC}$ calculations is provided in SI Text S3. Additionally, $Abs_{\lambda,BrC}$ was caused by primary and secondary BrC light absorption ($Abs_{\lambda,BrC,pri}$ and $Abs_{\lambda,BrC,sec}$). The $Abs_{\lambda,BrC,sec}$ value was calculated by a minimum R-squared (MRS) method at each wavelength (Wang et al., 2019; Wu and Yu, 2016; Wu et al., 2024). The detailed information of MRS method and $Abs_{\lambda,BrC,sec}$ estimation is provided in SI Text S3.

The multiple linear regression (MLR) method was used to analyze the light absorption of different OA components at each wavelength: $Abs_{BrC}=a\times[OOA]+b\times[BBOA]+c\times[CCOA]+d\times[aqSOA]+e\times[HOA]$ (Qin et al., 2018; Xie et al., 2019). The [OOA], [BBOA], [CCOA], [aqSOA], and [HOA] indicated the mass concentrations of OA species; the a–e were constants, used to optimize the Abs_{λ} of each OA component, and equivalent to MAC values at each wavelength (i.e., a–e at 370 nm represented $MAC_{370,OOA}$, $MAC_{370,BBOA}$, $MAC_{370,CCOA}$, $MAC_{370,aqSOA}$, and $MAC_{370,HOA}$, respectively). Here, the normalized mean bias (NMB), root mean square error (RMSE), and index of agreement (IOA) were used to evaluate the performance of the MLR method (SI Text S4) (Li et al., 2011). The IOA values of $Abs_{370,BrC}$ and $Abs_{470,BrC}$ (0.99 and 1.00) exceeded 0.95. The slopes of the relationship between $Abs_{370,BrC}$ and $Abs_{470,BrC}$ measured by AE33 and estimated by MLR method were 0.81 and 0.96 (close to unity), respectively. These results indicated a good agreement of $Abs_{370,BrC}$ between AE33 measurement and the MLR reconstruction.

3 Results and discussion

3.1 General descriptions

The temporal variations of $PM_{2.5}$ species concentrations, meteorological parameters, $Abs_{370,BrC}$ and $MAC_{370,BrC}$ during the campaign are shown in Fig. 1. The winds were weak with 0.3 ± 0.2 m s^{-1} over the whole campaign, indicating the atmosphere was in stagnant conditions. The total $PM_{2.5}$ (BC+NR-$PM_{2.5}$) mass concentrations ranged from 7.0 to 175.5 μg m^{-3}, with an average of 48.4 ± 27.8 μg

253 m^{-3} during the campaign. The average concentrations of OA, NO_3, SO_4, NH_4, Chl,
254 and BC were 24.1 ± 18.1, 8.3 ± 6.2, 6.2 ± 3.4, 5.2 ± 2.7, 0.2 ± 0.1, and 4.7 ± 2.9 μg
255 m^{-3}, taking up 46.6 ± 10.7%, 17.7 ± 8.0%, 13.2 ± 4.4%, 11.2 ± 2.7%, 0.3 ± 0.2%, and
256 10.1 ± 5.5% of total $PM_{2.5}$, respectively. OA constituted the largest fraction of total
257 $PM_{2.5}$, highlighting the importance of OA in $PM_{2.5}$ pollution in SCB (Bao et al., 2023;
258 Wang et al., 2018). Meanwhile, the high values of $Abs_{370,BrC}$ and $MAC_{370,BrC}$, ranging
259 from 5.8 to 210.2 Mm^{-1} (42.4 ± 28.5 Mm^{-1}) and from 0.6 to 7.0 m^2 g^{-1} (2.1 ± 0.9 m^2
260 g^{-1}) respectively, were observed during the campaign.

261 According to the Chinese National Ambient Air Quality Standard (NAAQS) (GB
262 3095-2012) (MEP, 2012), the Grade I annd Grade II levels for daily $PM_{2.5}$ mass
263 concentration are 35 μg m^{-3} and 75 μg m^{-3}, respectively. The Chinese NAAQS Grade
264 II level, based on WHO's Phase-1 interim target (IT-1), is higher than the WHO Air
265 Quality Guideline (AQG) value (15 μg m^{-3}), the EU daily limit (25 μg m^{-3}), and U.S.
266 24-hour standard (35 μg m^{-3}). During the campaign, the average of $PM_{2.5}$ mass
267 concentration was 1.4 times NAAQS Grade I level (35 μg m^{-3}). Therefore, the
268 pollution periods (PP) were defined by the daily $PM_{2.5}$ mass concentration exceeding
269 NAAQS Grade II level of 75 μg m^{-3}. Similarly, the days with $PM_{2.5}$ mass
270 concentration below 75 μg m^{-3} were characterized as clean periods (CP). During PP,
271 the mass concentrations of BC+NR-$PM_{2.5}$ and OA were 102.3 ± 26.9 and 57.4 ± 22.5
272 μg m^{-3}, 2.5 and 3.1 times that during CP, respectively. As shown in Fig. 2, the $PM_{2.5}$
273 species were substantially different in the PP and CP. Compared with other species, a
274 significantly higher contribution of OA was observed during PP (56.6%) than CP

(46.6%) (Student's t-test, $p < 0.001$) (Fig. 2). Here, five OA factors were identified by the PMF model with detailed information in SI Text S1, and the mass spectrum of these factors is shown in Fig. S9. HOA mass spectrum was characterized by alkyl fragment ion series at $C_nH^+_{2n-1}$ and $C_nH^+_{2n+1}$ (i.e., m/z 41, 43, 55, and 57), they are common characteristics of primary combustion emissions (Elser et al., 2016; Lanz et al., 2007). BBOA was identified by the high signal of m/z 60 (mainly $C_2H_4O_2^+$) and m/z 73 (mainly $C_3H_5O_2^+$), they are the fragments of levoglucosan and mannosan emitted from incomplete biomass burning (Alfarra et al., 2007). CCOA had high correlation with the unsaturated hydrocarbon ion fragments such as PAH-related ion fragments (i.e., m/z 77, 91, 115), emitted from traditional coal combustion (Sun et al., 2016a). OOA was distinguished by the prominent signal of m/z 44 (mainly CO_2^+) and highly correlated with the oxygenated ions (Ng et al., 2011b). aqSOA also had high correlation with the the oxygenated ions (i.e, m/z 43 (mainly $C_2H_3O^+$) and m/z 44). Moreover, The mass spectrum of aqSOA showed a significantly higher m/z 29 (mainly CHO^+) signal than other OA factors, consistent with those reported in the previous studies (Sun et al., 2016a; Xu et al., 2019; Zhao et al., 2019; Zhong et al., 2021). Moreover, BBOA showed significant correlations with m/z 60 (mainly $C_2H_4O_2^+$) and m/z 73 (Pearson's r^2 (r^2) = 0.85, 0.80, $p < 0.001$); CCOA was strongly correlated with Chl and m/z 115 (r^2 = 0.56, 0.48, $p < 0.001$); HOA was correlated with NO_2 and m/z 41 (r^2 = 0.47, 0.59, $p < 0.001$); OOA and aqSOA were significantly correlated with NO_3, NH_4 (r^2 = 0.77, 0.75, $p < 0.001$) and SO_4, ALWC (r^2 = 0.67, 0.85, $p < 0.001$), respectively (Fig. S10). These results highlighted the result of five OA

297 factors was reasonable.

298 It should be noted that the contributions of BBOA and aqSOA to OA increased
299 from CP (31.7% and 12.6%) to PP (38.6% and 14.1%), while CCOA, HOA, and OOA
300 contributions decreased. Additionally, significantly higher RH and ALWC were
301 observed during PP (58.5 ± 12.4% and 69.4 ± 30.3 μg m^{-3}) than CP (49.8 ± 8.9% and
302 37.1 ± 20.8 μg m^{-3}) ($p < 0.001$), but not temperature ($p > 0.1$). The wind was 0.32 ±
303 0.18 m s^{-1} during CP, 1.3 times that during PP. These results indicated that the
304 atmosphere was in a stagnant state with relatively high RH and ALWC during PP,
305 which might lead to the largely different sources and chemical processing of OA
306 during CP and PP. Compared with CP, the obvious diurnal variation of OA
307 concentration was exhibited during PP. As shown in Fig. 2, the OA concentration peak
308 (82.7 μg m^{-3}) was observed at 12:00 local time (LT) in the daytime during PP, while
309 observed at 21:00 LT at night during CP. Moreover, OA concentration rapidly
310 increased at a rate of 7.8 μg m^{-3} hr^{-1} from 09:00 to 12:00 LT with a significant
311 decrease of NO_3 during PP. Meanwhile, BBOA and aqSOA concentrations showed
312 similar diurnal patterns to OA concentration with high values in the daytime and
313 rapidly increased from 09:00 to 12:00 LT during PP. Previous research indicated that
314 aqSOA spectrum showed higher m/z 29 (CHO^+) than other OA factors (Gilardoni et
315 al., 2016; Meng et al., 2020; Wang et al., 2021). During PP, the peaks of m/z 60 and
316 m/z 29 concentrations, tracer ion fragments of BBOA and aqSOA, were observed at
317 12:00 LT (1.2 μg m^{-3}) and 13:00 LT (4.3 μg m^{-3}), respectively. Additionally, the
318 correlation between ALWC and aqSOA concentrations ($r^2 = 0.86$, $p < 0.001$) was

stronger than BBOA concentrations (r^2 = 0.58, p < 0.001), and both ALWC and aqSOA concentration peaks were observed at 13:00 LT, earlier than BBOA concentration peak (12:00 LT), supporting that ALWC might play a significant role in the chemical processing of aqSOA formation from BBOA during PP. In contrast, the odd oxygen ($O_x = O_3 + NO_2$) showed weak correlations with both OOA and aqSOA concentrations during the campaign (p > 0.1) (not shown). Although the average O_x concentration was higher during PP (51.1 ± 19.6 ppb) than CP (36.9 ± 14.0 ppb), no significant correlations were observed in either period (not shown). These results suggested that photochemical reactions might played a limited role in SOA formation in this study.

In summary, these results suggested that OA was the dominant component of $PM_{2.5}$, especially during PP in SCB. During PP, BBOA and aqSOA played important roles in increasing OA concentration in the daytime. Additionally, considerable aqSOA in the daytime during PP might be related to the high aerosol water and BBOA emissions in the harvest season − autumn − in SCB (Bao et al., 2023; Chen et al., 2017; Chen et al., 2019; Tao et al., 2014). Based on the direct observation of aqSOA, Gilardoni et al. (2016) also found that aqSOA such as guaiacol dimer ($C_{14}H_{14}O_4^+$) could be formed from aged biomass-burning emissions at both in fog water and in wet aerosol, especially under high ALWC conditions. To further explore aqSOA formed from biomass-burning emissions via the aqueous-phase reactions, the next section would discuss the dynamic evolution of aqSOA in relation to BBOA.

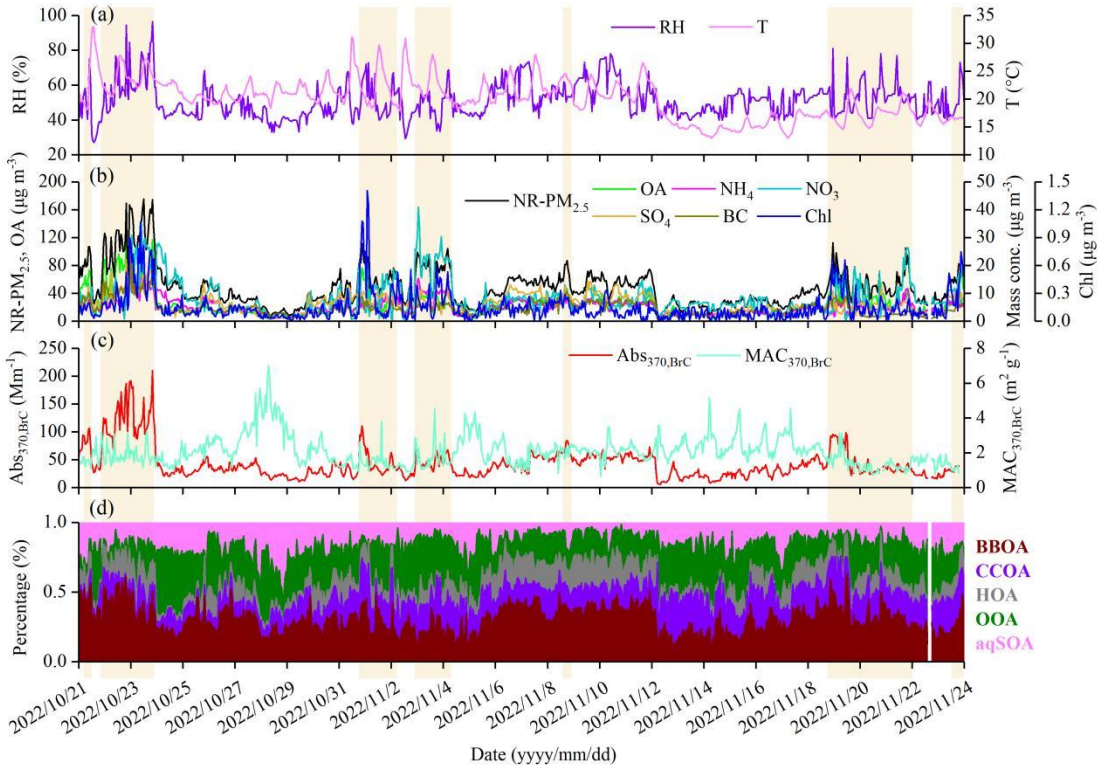

340

341 **Figure 1.** Time series of **(a)** RH and T, **(b)** NR-$PM_{2.5}$ species measured by ToF-ACSM and BC, **(c)**

342 $Abs_{370,BrC}$ and $MAC_{370,BrC}$, and **(d)** mass fraction of OA factors during the campaign. The pollution

343 period (BC+NR-$PM_{2.5}$ > 75 μg m^{-3}) is highlighted by the shaded areas.

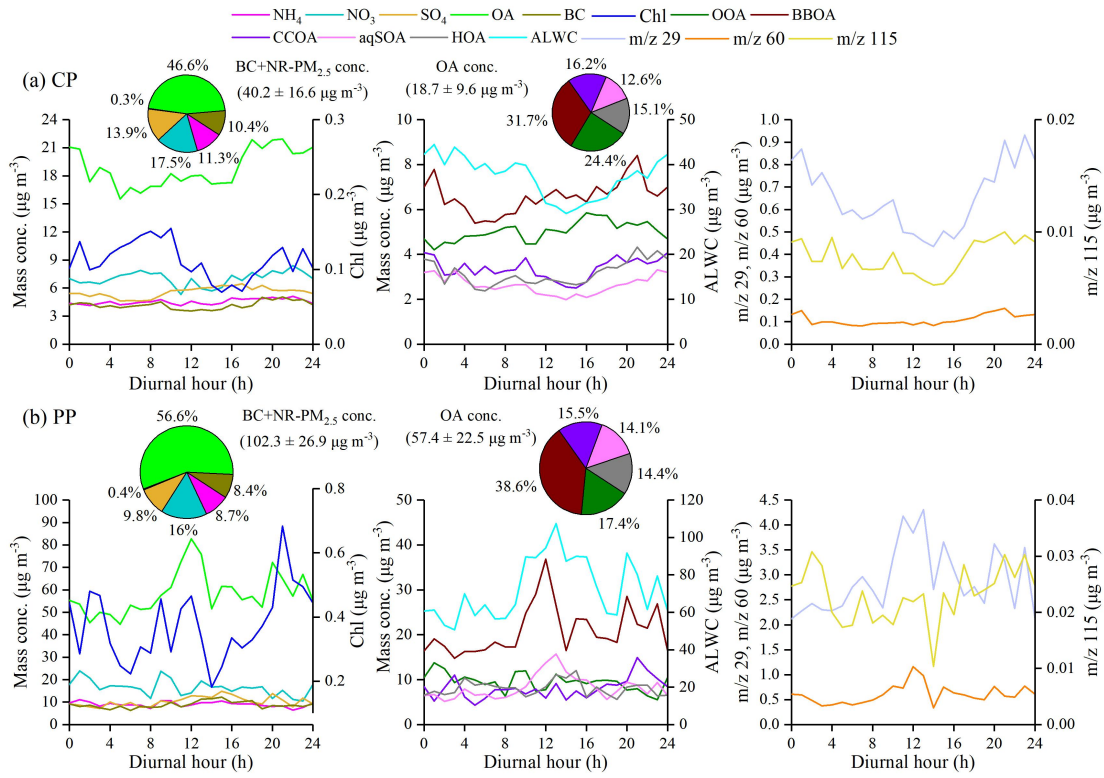

344

Figure 2. Diurnal variations of $PM_{2.5}$ species, BC, OA factors, m/z 29, m/z 60, and m/z 115 mass concentrations during **(a)** clean period (CP) (BC+NR-$PM_{2.5}$ < 75 μg m^{-3}) and **(b)** polluted period (PP) (BC+NR-$PM_{2.5}$ > 75 μg m^{-3}). The pie charts in the left side of **(a)** and **(b)** show the average mass contributions of different chemical compositions to BC+NR-$PM_{2.5}$ during CP and PP, respectively. Meanwhile, the average mass contributions of OOA, BBOA, CCOA, aqSOA, and HOA in OA are shown in the pie charts in the middle of **(a)** and **(b)**, respectively.

3.2 Biomass-burning emissions as precursors for aqSOA

Fig. 3 shows the strong correlation between the mass fraction (%) of aqSOA in total $PM_{2.5}$ and ALWC during the campaign (r^2 = 0.64, p < 0.001). The contribution of aqSOA increased with the increase of f_{29} values (normalized mass spectrum signal at m/z 29). It was important to note that the aqSOA factor showed significantly higher f_{29} and f_{60} values (normalized mass spectrum signal at m/z 60) (0.167 and 0.011) than the OOA factor (0.017 and 0.002), respectively (Fig. S9). Moreover, both aqSOA concentrations and f_{29} were well correlated with ALWC (r^2 = 0.85, 0.73, p < 0.001) (Fig. 3). During the campaign, the average value of the oxygen-to-carbon ratio (O:C) of aqSOA factor (0.85) was 2.7 times that (0.31) of BBOA factor. However, the similar hydrogen-to-carbon ratio (H:C) values of aqSOA factor and BBOA factor were observed (1.74 and 1.81, respectively), indicating that a hydrogen atom might be replaced by a OH moiety (Lim et al., 2010; Ng et al., 2011a). These results were similar to aqSOA observed in Italy and Beijing (Gilardoni et al., 2016; Zhao et al., 2019). Additionally, previous studies indicated that aqueous-phase processes could

play a role in the formation of SOA from fossil fuel emissions (Ervens et al., 2011; Huang et al., 2023; Wang et al., 2021; Xu et al., 2022; Yan et al., 2017). For example, Wang et al. (2021) and Xu et al. (2022) have highlighted the potential for aqueous-phase reactions to contribute to SOA formation, particularly in regions with high levels of anthropogenic emissions. In this study, a strong anticorrelation between the mass fraction of fossil-fuel related OA components (sum of CCOA, HOA and OOA) and ALWC at the high f_{29} values was also observed (r^2 = 0.48, p < 0.001) (not shown), consistent with recent research (Wang et al., 2021). This indicated that aqSOA might also be produced by aqueous-phase reactions of fossil-fuel related OA components.

Fig. 4 shows the relationships between ALWC and OA factors or f_{29} during the campaign. Five OA factors mass concentrations increased with the increase of ALWC. However, compared with other OA factors, aqSOA and BBOA significantly increased from 1.1 and 4.9 μg m^{-3} to 5.2 and 10.8 μg m^{-3} when 20 μg m^{-3} < ALWC < 60 μg m^{-3}, respectively. It should be noted that only aqSOA concentrations were enhancement under high ALWC conditions (> 100 μg m^{-3}). It is likely because more water-soluble organic species (i.e., glyoxal and methylglyoxal) were formed, that were further oxidized to form aqSOA via aqueous-phase reactions in aerosol liquid water (Carlton et al., 2007; Ervens et al., 2011; Tan et al., 2012). As shown in Fig. 4b, the mass fraction of aqSOA showed significant enhancement from less than 5% at ALWC < 20 μg m^{-3} to 17−22% at ALWC > 60 μg m^{-3} with a corresponding decrease in OOA, although POA (BBOA+CCOA+HOA) and SOA (OOA+aqSOA)

contributions were fairly constant across different ALWC levels (58−68% and 32−42%). This result suggested a more intensive formation of aqSOA than OOA via aqueous-phase reactions, although aqSOA might be also formed from OOA, consistent with the recent research in northwest China (Zhao et al., 2019; Zhong et al., 2021). Additionally, the increasing f_{29} (CHO^+) from 0.010 to 0.227 as a function of ALWC was observed during the campaign (Fig. 4b). The values of f_{29} significantly increased from 0.055 to 0.210 when ALWC increased from 60 μg m^{-3} to 100 μg m^{-3} ($p < 0.001$), consistent with OA mass concentrations (13.2−109.1 μg m^{-3}) during the campaign (Fig. 4b). According to the laboratory analysis of organic standards, previous research found that the spectra of standard organic species without alcohol group showed low f_{29} (< 0.05), while high f_{29} values (0.05–0.15) were found for polyols and species with non-acid OH groups produced from biomass-burning emissions (Canagaratna et al., 2015; Gilardoni et al., 2016; Zhao et al., 2014). This further highlighted the potential formation of organic compounds with hydroxyl groups (i.e., glyoxal and methylglyoxal) under high ALWC conditions. Overall, these results pointed to the fact that the observed aqSOA could be formed from biomass-burning emissions via aqueous-phase reactions, reinforcing the BBOA role in increasing $PM_{2.5}$ mass concentration.

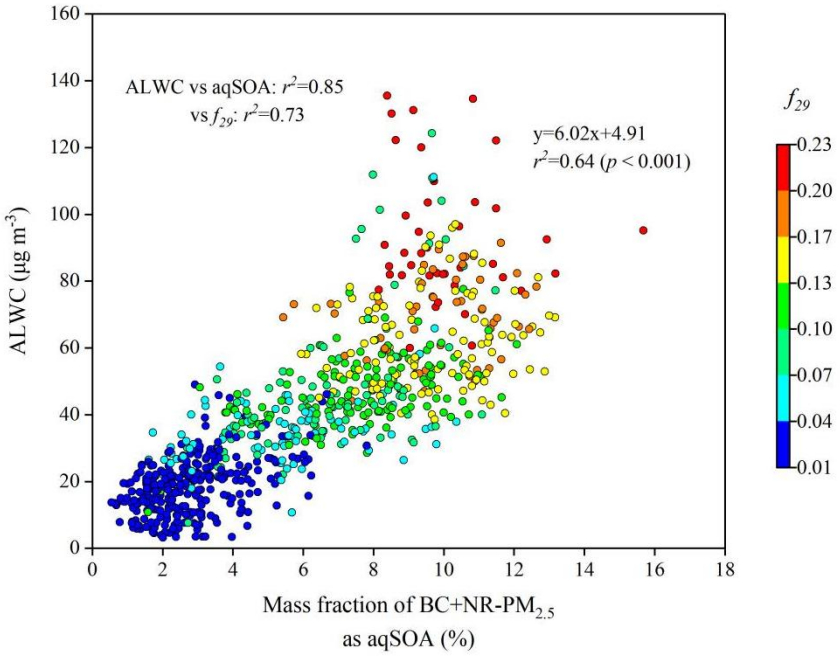

406

407 **Figure 3.** Scatter plot of the mass fraction of aqSOA in BC+NR-$PM_{2.5}$ versus ALWC colored by

408 the f_{29} (normalized mass spectrum signal at m/z 29) during the campaign. f_{29} (mainly CHO^+) is a

409 tracer for alcohol compounds and used to monitor the aqueous-phase oxidation of organic

410 compounds (i.e., glyoxal).

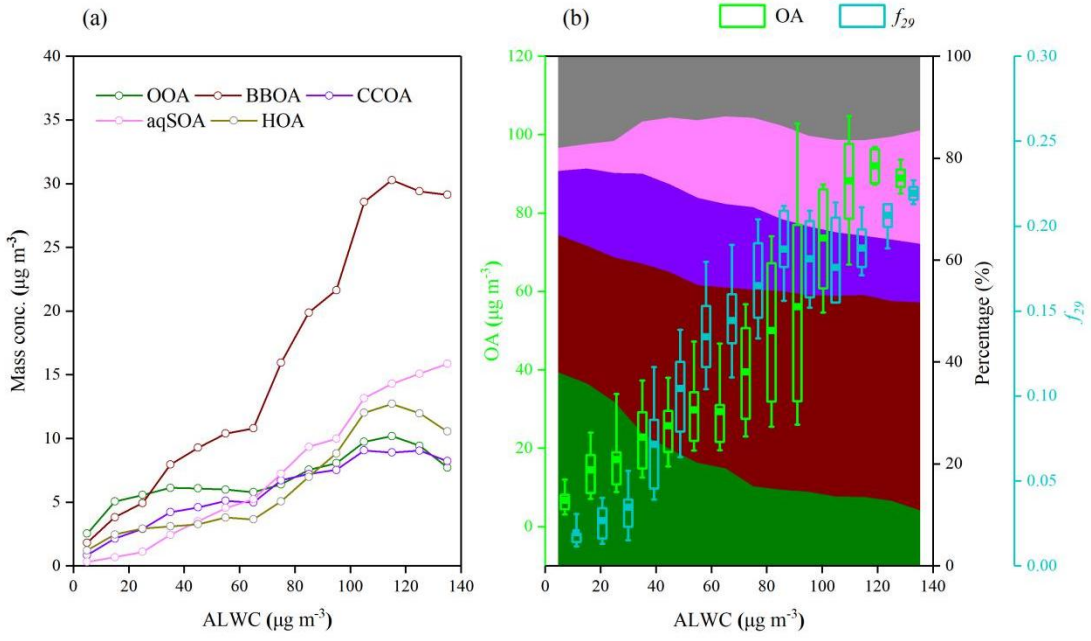

411

412 **Figure 4.** Variations of **(a)** OA factors mass concentrations, and **(b)** OA mass concentrations, f_{29} (a

413 tracer for alcohol compounds), and mass fraction of OA factors as a function of ALWC. The data

414 were grouped into different bins according to a 10 μg m^{-3} increment of ALWC.

415 To identify the formation of aqSOA and its precursors under different $PM_{2.5}$
416 pollution levels, the relationship between aqSOA and BBOA or OOA mass
417 concentrations with ion fragments tracers during CP and PP was performed,
418 respectively. The correlation r^2 between aqSOA and BBOA concentrations was
419 higher during PP (0.64) than that during CP (0.54) ($p < 0.001$) (Fig. 5a and c). Though
420 aqSOA and BBOA concentrations increased with the increase of ALWC during CP
421 and PP, the correlations between ALWC and aqSOA or BBOA concentrations were
422 relatively stronger during PP than that during CP ($p < 0.001$). Fig. 5b and d show that
423 f_{29} was highly correlated with aqSOA formation during CP and PP. A few data points
424 with high aqSOA and OOA concentrations had low f_{29} values (0.071−0.102) in Fig. 5d,
425 while the average value of f_{44} (normalized mass spectrum signal at m/z 44) of these
426 data points (0.103 ± 0.024) was 1.3 times that of all data points (0.080 ± 0.035) during
427 PP. It was likely due to the formation of more-oxidized OOA under high ALWC
428 values (> 80 μg m^{-3}) in this study (Xu et al., 2017). Previous research found that the
429 f_{29} values of polyols and species with non-acid OH groups from biomass-burning
430 emissions were lower than 0.15 (Canagaratna et al., 2015; Gilardoni et al., 2016; Zhao
431 et al., 2014). Moreover, the mass fraction of aqSOA showed a stable increasing trend
432 and remained high levels (from 18% to 22%) at ALWC > 80 μg m^{-3}, which was
433 associated with a corresponding decrease in OOA (from 15% to 10%) (Fig. 4b).
434 Compared with OOA ($p > 0.1$), the aqSOA concentrations showed strong positive
435 correlation with ALWC ($r^2 = 0.73$, $p < 0.001$) when ALWC > 80 μg m^{-3} during PP. In

436 contrast, ALWC showed the weak correlations with aqSOA and OOA concentrations
437 during CP ($p > 0.1$). It should be noted that a strong anticorrelation between aqSOA
438 and OOA concentrations was observed during PP at ALWC > 80 μg m^{-3} when f_{29} >
439 0.15 ($r^2 = 0.76$, $p < 0.001$), but not during CP ($p > 0.1$) (Fig. 5b and d). These results
440 indicated that the aqSOA formation was more intensive than OOA at high ALWC
441 levels during PP.

442 Previous research demonstrated that f_{44} (representation of aged OA) could be
443 used as a tracer of aged SOA, f_{43} (normalized mass spectrum signal at m/z 43) as a
444 tracer of POA and fresh SOA, and f_{60} (presence of anhydrosugars) as a tracer of
445 BBOA (Cubison et al., 2011; Ng et al., 2010). Additionally, m/z's 44 and 43 are
446 usually from different functional groups and the ratio changes as a function of
447 atmospheric aging. The triangle plot of f_{44} versus f_{43} has been widely used to
448 characterize OA evolution, and f_{44} versus f_{60} is commonly used to investigate the
449 aging trend of BBOA (Ortega et al., 2013; Paglione et al., 2020; Xu et al., 2017; Xu et
450 al., 2019). As shown in Fig. 6, the bottom region of the triangle was dominated by
451 BBOA, CCOA, and HOA with low f_{44} (0.040, 0.017, and 0.016, respectively) in this
452 study, indicating that they were freshly emitted and less oxidized. However, the f_{44} of
453 SOA factors (i.e., OOA and aqSOA) (0.118 and 0.117) were observably higher than
454 POA factors, showing the freshly oxidized properties of SOA. Meanwhile, f_{44} of
455 aqSOA was close to that observed in fogs (Gilardoni et al., 2016; Kim et al., 2019),
456 highlighting the presence of aqueous-phase reactions in this study. The relative
457 abundance of m/z 45 (mainly HCO_2^+), a tracer ion for carboxylic acids, was higher in

458 the aqSOA spectra than in the OOA spectrum (Fig. S9). It was consist with previous
459 research which found that aqueous-phase reactions were important sources of
460 oxygenated organic compounds, including organic acids (Ervens et al., 2011; Kim et
461 al., 2019; McNeill, 2015; Sun et al., 2010; Yu et al., 2014). Fig. 6b shows BBOA and
462 aqSOA with higher f_{60} values (0.019 and 0.011) than CCOA (0.009) and HOA (0.008).
463 The f_{60} value of OOA was 0.002, lower than the typical background value (0.003) in
464 the atmospheric without biomass burning influence (Cubison et al., 2011). The mass
465 spectrometry feature of aqSOA showed large f_{44} and f_{60} values, laying in a schematic
466 space of aged BBOA based on mass spectrometry features in previous research
467 (Cubison et al., 2011; Ortega et al., 2013). Additionally, BBOA contains abundant
468 water-soluble organic compounds (WSOC) with (i.e., sugars, phenols, and organic
469 acids), that can form aqSOA via efficient aqueous-phase reactions (i.e., oxidation and
470 oligomerization reactions) (Ervens et al., 2011; Gilardoni et al., 2016; Lee et al., 2013;
471 Lei et al., 2024; Li et al., 2020; Powelson et al., 2014). In contrast, OOA formation
472 primarily relies on gas-phase oxidation of VOCs with high-reactivity (i.e., aromatics
473 and long-chain alkanes) (i.e., OH radicals), which has low concentrations in BBOA
474 (Akagi et al., 2011; Jimenez et al., 2009; Shrivastava et al., 2017; Yokelson et al.,
475 2007). This suggested that BBOA could be the important precursors for aqSOA
476 instead of OOA via aqueous-phase reactions. These results were consistent with
477 previous research and most of the observation data were within the triangle space
478 (Bao et al., 2023; Kim et al., 2019; Paglione et al., 2020).

During PP, the f_{44} values ranging from 0.022 to 0.140 (0.080 ± 0.035) were significantly higher than that during CP (0.021−0.150, 0.064 ± 0.019) ($p < 0.001$), while the f_{43} value was slightly lower with an average of 0.062 ± 0.027. Compared with CP ($r^2 = 0.17$, slope = −0.53), f_{44} showed a more significant increase as the decreasing of f_{43} with higher r^2 value (0.70) and the regression slope of f_{44} versus f_{43} (−1.09) was closer to −1 during PP. This indicated that more aged SOA existed in the atmosphere during PP (Fig. 6a and c). It should be noted that the points of f_{44} versus f_{43} were inside the upper boundary of the triangle region, and most points were outside the bottom boundary of the triangle region during PP. These results suggested that less oxidized SOA were formed via aqueous-phase reactions instead of photo-chemical reactions during PP (Kim et al., 2019; Zhao et al., 2019). Moreover, these points outside the bottom boundary of the triangle region with higher f_{44} (> 0.05) and lower f_{43} (< 0.06) showed relatively higher ALWC during PP, but not during CP.

Here, the triangle plots of f_{44} versus f_{60} colored by ALWC under different $PM_{2.5}$ pollution levels were analyzed (Fig. 6b and d), when the link between aqSOA and BBOA was further stressed by a schematic representation of aged BBOA. Except for several points, the f_{60} values were ubiquitously higher than 0.003, and most points fell in the triangular region, suggesting the contribution of biomass burning to OA. During PP, the f_{60} values ranging from 0.005 to 0.019 (0.010 ± 0.004) were similar with CP (from 0.004 to 0.019, 0.010 ± 0.003). The correlation r^2 between f_{44} and f_{60} was higher during PP (0.72) than that during CP (0.31) ($p < 0.001$). Moreover, compared with all data points during PP, those in the schematic space of aged BBOA showed relatively

501 higher ALWC, a pattern that differed from observations during CP.

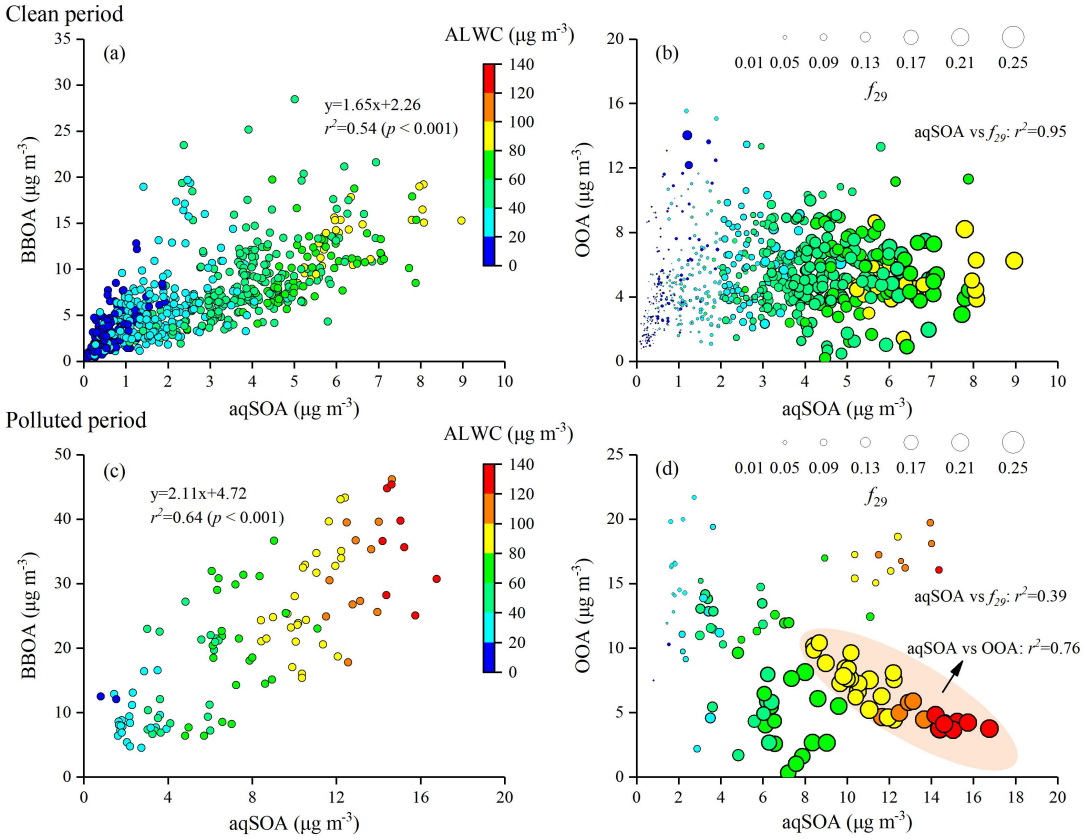

502

503 **Figure 5.** Scatter plots of aqSOA versus **(a, b)** BBOA and **(c, d)** OOA mass concentrations

504 colored by ALWC during clean period and polluted period. The size of the symbols in **(b)** and **(d)**

505 increases with the increase of the f_{29} value, which is a tracer for alcohol compounds.

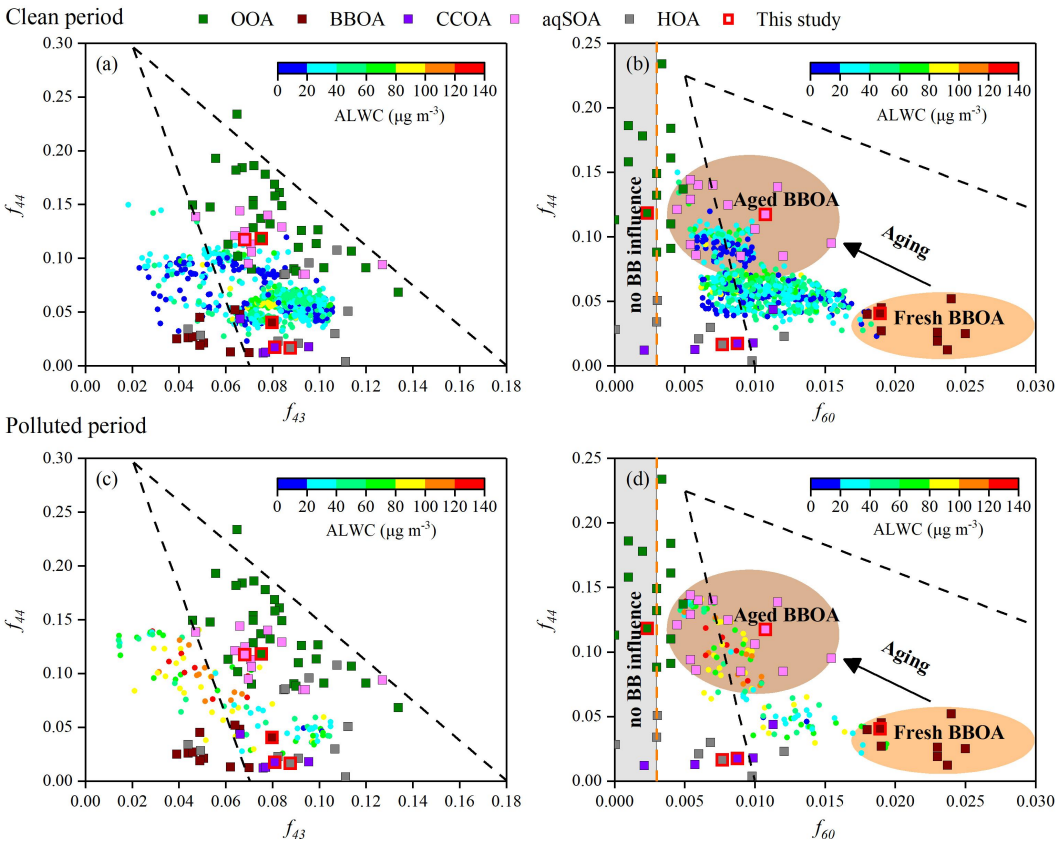

Figure 6. Triangle plots of **(a, c)** f_{44} (normalized mass spectrum signal at m/z 44) versus f_{43} (normalized mass spectrum signal at m/z 43), and **(b, d)** f_{44} versus f_{60} (normalized mass spectrum signal at m/z 60) colored by ALWC (circles) during clean period and polluted period. The dashed lines in **(a)** and **(c)** were derived from Ng et al. (2010) and used to follow the aging of OA components in the atmosphere. The background space (f_{60} < 0.003) without biomass burning influence was also shown by the grey shaded area. The background value of secondary aged OA (brown dashed line) and the black dashed lines characterising the aging of BBOA in **(b)** and **(d)** were derived from Cubison et al. (2011). The data points (squares) included the measurements in this study (bordered in red) and previous research (Bao et al., 2023; Gilardoni et al., 2016; Kim et al., 2019; Ng et al., 2011a; Paglione et al., 2020; Xu et al., 2015; Xu et al., 2017; Xu et al., 2019; Zhao et al., 2017; Zhao et al., 2019). f_{43} (mainly $C_2H_3O^+$) is a tracer for POA and fresh SOA. f_{44} is a proxy of the OA oxygenation degree and used as a tracer for aged SOA. f_{60} is a proxy of

519 anhydrosugars emitted from biomass burning.

520 **3.3 Evolution of BrC Absorption**

521 Previous research indicated that OA from fresh and aged biomass-burning
522 emissions, which exhibited absorption properties across UV to Vis range with
523 significantly higher AAE value than BC, might contribute to a net positive radiative
524 forcing (Laskin et al., 2015). Therefore, the BrC absorption properties and their
525 relationship with five OA factors were analyzed in this study. The values of $Abs_{\lambda,BrC,pri}$
526 and $Abs_{\lambda,BrC,sec}$ were obtained by MRS method, and the MLR method was used to
527 estimate Abs of five OA factors at each wavelength (SI Text S3 and S4). The average
528 value of $Abs_{370,BrC}$ was 42.4 ± 28.5 Mm^{-1} (accounting for 49.2% of Abs_{370}), much
529 higher than $Abs_{660,BrC}$ (2.6 ± 1.3 Mm^{-1}, 10.5%), suggesting a high absorption
530 efficiency for BrC in the near-UV wavelength. The $Abs_{\lambda,BrC,pri}$ and $Abs_{\lambda,BrC,sec}$
531 accounted for 56.8%−72.5% and 27.5%−43.2% of $Abs_{\lambda,BrC}$ from 370 nm to 660 nm
532 respectively, indicating primary emissions were the main contributors to BrC
533 absorption (Fig. S12). However, the contribution of $Abs_{\lambda,BrC,sec}$ to $Abs_{\lambda,BrC}$ increased
534 with wavelength, suggesting the impact on Abs_{BrC} from SOA should not be ignored.
535 Hereafter, we show that aqSOA formation from aged BBOA contributed to the BrC
536 budget and was strong absorption across UV to Vis range.

537 The data at 370 nm with higher signal-to-noise ratios and Abs_{BrC} contribution
538 was chosen to further analyze the correlations of BrC absorption with various OA
539 components. As described in section 2.3.3, the Abs of five OA factors at each

wavelength were obtained by the MLR method (Table S1). Compared with CCOA ($Abs_{370,CCOA}$), HOA ($Abs_{370,HOA}$), and OOA ($Abs_{370,OOA}$) (11.5%, 9.1%, and 11.1%), the Abs at 370 nm calculated for BBOA ($Abs_{370,BBOA}$) and aqSOA ($Abs_{370,aqSOA}$) showed higher contributions (51.9% and 16.4%) to $Abs_{370,BrC}$, consistent with the higher MAC values (Fig. S14). Fig. S15 presents the correlations between $Abs_{370,BrC}$ and the mass concentrations of OOA, BBOA, CCOOA, aqSOA, HOA, and m/z 60. $Abs_{370,BrC}$ showed the strongest positive correlations with BBOA and m/z 60 (ion fragments tracers of BBOA) concentrations (r^2 = 0.77, p < 0.001), followed by aqSOA concentrations (r^2 = 0.69, p < 0.001). In contrast, the correlations with HOA concentrations (r^2 = 0.36), CCOA (r^2 = 0.25), and OOA (r^2 = 0.09, p > 0.1) were much weaker. Compared with other OA factors (except BBOA), the contribution of $Abs_{370,aqSOA}$ to $Abs_{370,BrC}$ was relatively higher (Table S1), when the correlation between $Abs_{370,BrC}$ and aqSOA concentrations was also stronger. These results might be related to the aqSOA formed from the aged BBOA via aqueous-phase reactions. Gilardoni et al. (2016) demonstrated that aqSOA formation from aged BBOA via aqueous-phase reactions in the ambient atmosphere contributed to the BrC budget and exhibited slightly higher $AAE_{467–660}$ (AAE of aerosols from 467 nm to 660 nm) values than the fresh and processed biomass-burning emissions in laboratory experiments. The MAC values of the five resolved OA components equivalent to the a–e values in the MLR method at different wavelengths were shown in Fig. S14. Among these, BBOA showed the highest MAC value (2.37 m^2 g^{-1}), followed by aqSOA (1.23 m^2 g^{-1}) at 370 nm, indicating that the oxidation of BBOA to aqSOA

562 decreased light absorption at short wavelengths. Previous research found that the
563 MAC of BBOA at 365 nm was twice that of SOA, which was associated with the
564 water-soluble BrC (Lorenzo et al., 2017; Washenfelder et al., 2015). The AAE values
565 of OA factors, calculated by a power-law fitting of Abs for these OA factors from 370
566 nm to 660 nm (Qin et al., 2018; Wang et al., 2019), were shown in Fig. S14. It should
567 be noted that aqSOA had the lowest $AAE_{370-660,aqSOA}$ value (3.54), while BBOA has
568 the highest $AAE_{370-660,BBOA}$ value (4.93). Moreover, the contribution of aqSOA to
569 Abs_{BrC} increased from 16.4% to 26.7% from 370 to 660 nm, while the contribution
570 from BBOA decreased from 51.9% to 39.1% from 370 to 660 nm. These suggested
571 aqSOA formation from aged BBOA might play an important role in the light
572 absorption of BrC across UV to Vis range.

573 Fig. 7 shows the ternary contour map to quantify the contribution of BBOA,
574 CCOA, and HOA factors to $Abs_{370,BrC,pri}$, when the strong positive correlation ($p <$
575 0.001) and high slope of the linear regression (1.80) between BBOA mass
576 concentrations and $Abs_{370,BrC,pri}$ were observed. Among these POA factors, the high
577 mass fractions of BBOA to POA were consistent with the high $Abs_{370,BrC,pri}$ values
578 (Fig. 7a). For example, the most data of $Abs_{370,BrC,pri}$ higher than 49.1 Mm^{-1} (90th
579 percentile of $Abs_{370,BrC}$) fell in the region of high BBOA/POA values (> 0.5).
580 Moreover, $Abs_{370,BrC,pri}$ significantly increased with the increases of BBOA and m/z 60
581 mass concentrations with higher r^2 values (0.63 and 0.55) than HOA and CCOA (0.19
582 and 0.14) (Fig. 7b). These results indicated the major contribution of BBOA to
583 primary BrC light absorption.

584 During the campaign, the relationship between $Abs_{370,BrC,sec}$ and SOA factors
585 mass concentrations was analyzed to understand the correlation between secondary
586 BrC absorption and its chromophores. As shown in Fig. S16, $Abs_{370,BrC,sec}$ significantly
587 increased with the increase of aqSOA concentrations (r^2 = 0.44, p < 0.001) and high
588 $Abs_{370,BrC,sec}$ values were consistent with the high ALWC values, this was not the case
589 for OOA (p > 0.1). The slope of the linear regression (3.50) between aqSOA mass
590 concentrations and $Abs_{370,BrC,sec}$ was higher than OOA (Fig. S16), so was the MAC
591 values of aqSOA across UV to Vis range (Fig. S14). To further characterize the
592 evolution of secondary BrC absorption, $Abs_{370,BrC,sec}$ was normalized by ΔCO (the
593 background-corrected CO mixing ratios) to minimize the effect of boundary layer
594 height (Fig. 8) (DeCarlo et al., 2010). Here, the background CO value (400 ppb) was
595 defined as the lowest 1.25th percentile of the CO values during the campaign (Kondo
596 et al., 2006). Fig. 8 shows that the values of $Abs_{370,BrC,sec}$/ΔCO increased with the
597 increases of aqSOA and ALWC concentrations from 17:00 to 03:00 LT (r^2 = 0.63,
598 0.57, p < 0.001), while $Abs_{370,BrC,pri}$/ΔCO slightly decreased with the increases of
599 BBOA and m/z 60 concentrations (r^2 = 0.35, 0.33, p < 0.001). Additionally, the mass
600 concentrations of NO_3, NH_4, and NO_2 from 17:00 to 03:00 LT were 1.2, 1.2, and 1.3
601 times that from 04:00 to 16:00 LT during the campaign. These results were similar to
602 those observed in SCB during winter (Peng et al., 2025; Wu et al., 2024). As
603 described in section 3.2, the SOA with hydroxyl groups (i.e., glyoxal and
604 methylglyoxal) could be formed from the aged BBOA via aqueous-phase reactions
605 under high ALWC during the campaign. Previous research have shown that oligomers

606 (involving two glyoxal molecules) formed via aqueous reactions of glyoxal with NH_3
607 contain C=C or C=N bonds, exhibiting strong absorption at near-UV (Laskin et al.,
608 2015; Lee et al., 2013; Nozière et al., 2009; Powelsonet al., 2014). This suggested
609 secondary BrC chromophores with strong absorption at 370 nm were formed under
610 the high ALWC from 17:00 to 03:00 LT, which might be related to the aqSOA from
611 the aged BBOA via aqueous-phase reactions. The low values of $Abs_{370,BrC,sec}/\Delta CO$ at
612 12:00−14:00 LT could be related to the photolysis and/or photooxidation causing BrC
613 photobleaching (Sareen et al., 2013; Zhao et al., 2015). Overall, we suggested that
614 aqSOA formed from biomass-burning emissions might be important for BrC
615 absorption, especially at night.

616 $AAE_{370–880}$ was another key parameter to characterize the absorption properties
617 of aerosols, its correlations with the mass fraction of aqSOA (f_{aqSOA}) and BBOA
618 (f_{BBOA}) to OA, and BC-to-OA ratios were shown in Fig. 9. During the campaign, the
619 strong positive correlation (r^2 = 0.49, p < 0.001) between $AAE_{370–880}$ and f_{aqSOA} was
620 observed with $AAE_{370–880}$ values up to 2.65, while $AAE_{370–880}$ values increased with
621 the slight increase of f_{BBOA} in general (r^2 = 0.21, p < 0.001) (Fig. 9a and c). AAE was
622 calculated using a power-law fitting of aerosol absorption values (Qin et al., 2018;
623 Wang et al., 2019). While BC concentration is linearly dependent on Abs_{BC}, OA
624 concentration does not follow the same pattern with Abs_{BrC}. The mixing state of BC
625 and OA, influenced by combustion conditions, can also affect AAE. Previous studies
626 have shown that biomass-burning emissions can impact absorption properties, which
627 is reflected in the relationship between AAE and the BC-to-OA ratio (a measure of the

combustion conditions) (Lu et al., 2015; Saleh et al., 2014). Thus, the relationship observed in Fig. 9b reflected the influence of biomass-burning emissions during the campaign, and the parameterized curve in this study (black) was consistent with prior research (red) using wavelengths from 370 nm to 880 nm (Lu et al., 2015). Here, 950 nm and 880 nm were used as the highest wavelength respectively, and similar values were found between $AAE_{370–950}$ and $AAE_{370–880}$ (within 10.0%). It should be noted that the data points of high $AAE_{370–880}$ were consistent with the low BC-to-OA ratios and large f_{aqSOA} values in general. Moreover, the average value of $AAE_{370–880}$ observed in this study (1.95) was higher than $AAE_{370–950}$ observed in the laboratory experiments of fresh and photo-chemically aged biomass-burning emissions (i.e., 1.38 and 1.48 for fresh oak and pocosin pine, 1.42 and 1.73 for aged oak and pocosin pine) (Saleh et al., 2013).

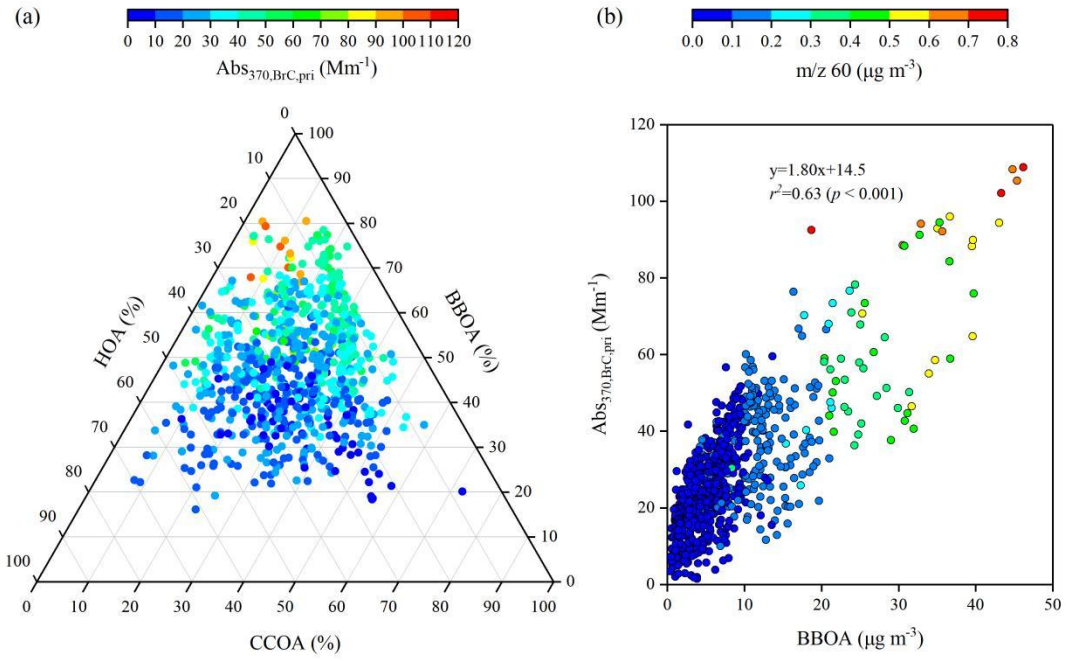

Figure 7. (a) Ternary diagram for the mass fractions of BBOA, CCOA, and HOA in POA colored by $Abs_{370,BrC,pri}$, and **(b)** scatter plot of BBOA mass concentrations versus $Abs_{370,BrC,pri}$ colored by m/z 60 mass concentrations.

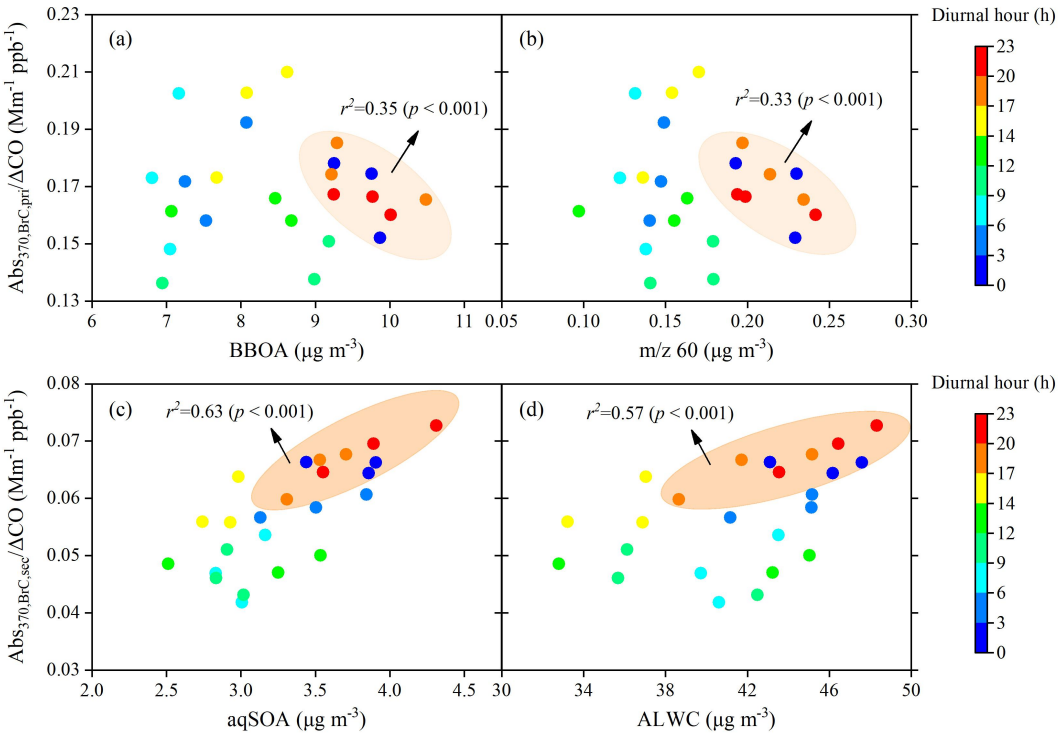

Figure 8. Scatter plots of $Abs_{370,BrC,pri}/\Delta CO$ versus **(a, b)** BBOA and m/z 60 mass concentrations and $Abs_{370,BrC,sec}/\Delta CO$ versus **(c, d)** aqSOA and ALWC colored by the local time.

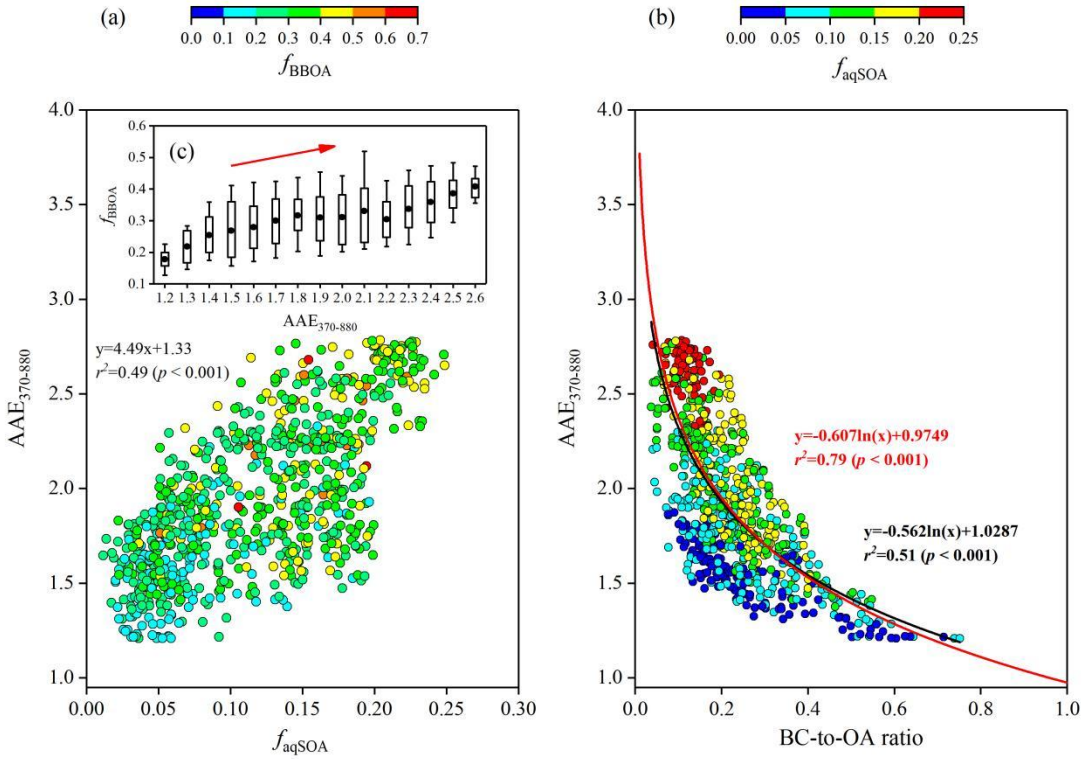

Figure 9. Relationship between **(a)** $AAE_{370–880}$ and the mass fraction of aqSOA (f_{aqSOA} = aqSOA/OA) colored by the mass fraction of BBOA (f_{BBOA} = BBOA/OA), and **(b)** BC-to-OA ratios colored by f_{aqSOA}. **(c)** Variations of f_{BBOA} as a function of $AAE_{370–880}$. The red curve in **(b)** was the best fit curve to data taken from Lu et al. (2015) and described the Abs of fresh and aged BBOA.

4 Conclusions

Field observations indicated that secondary organic aerosol (SOA) accounts for most of organic aerosol (OA) worldwide and aqueous-phase oxidation is an important pathway for the SOA formation. Our results demonstrated the fact that aqSOA was originated from the aged biomass-burning emissions via aqueous-phase reactions under high ALWC in the ambient atmosphere. Additionally, the less oxidized aqSOA formation via aqueous-phase reactions instead of photo-chemical reactions played a

key role in the haze pollution dynamic evolution during the polluted period. This study also indicated that the impact on secondary BrC absorption should not be ignored, although primary BrC dominated the BrC absorption across ultraviolet to visible range. The aqSOA formed from aged biomass-burning emissions significantly contributed to the BrC budget and showed stronger absorption across ultraviolet to visible range than other OA components (except BBOA). The similarity between ambient data and the parameterized curve of $AAE_{370–880}$ versus BC-to-OA ratios in this study was consistent with the previous laboratory research on biomass-burning emissions. Higher values of $AAE_{370–880}$ and $MAC_{\lambda,aqSOA}$ reinforced that aqSOA formation from aged biomass-burning emissions via aqueous-phase reactions had stronger absorption than that via photo-chemically reactions.

In conclusion, our results revealed the aqSOA formation and brownness from aged BBOA via aqueous-phase reactions and highlighted the importance of aqSOA on aerosol pollution and absorption in the Sichuan Basin, China. Brown aqSOA originating from biomass-burning emissions was an important player in air quality budget and climate forcing balance worldwide. And it should be taken into account in air quality and climate models for a correct description of the global OA budget and its climate-relevant optical properties. This study was helpful in understanding the formation, light properties, and impacts of aqSOA in the ambient atmosphere. Future research should focus on the molecular-level characterization, transportation, and reactivities of gas and particle-phase aqSOA precursors to improve understanding of aqSOA formation processes and absorption properties.

Data availability. The data generated and analysed in this study are available from https://doi.org/10.5281/zenodo.14626304 (Peng et al., 2025).

Author contributions. CZ, CP, YD, and ZL designed the experiments. Data analysis and interpretation were performed by CP, ZT, HT, KZ, ZL, and GS. CP, XY, and MT wrote the paper. ZT, YC, XL, LZ, YC, and YF contributed to the paper with useful scientific discussions or comments.

Competing interests. The authors declare that they have no conflict of interest.

Acknowledgements. This study was supported by the Natural Science Foundation of Chongqing Municipality (No. CSTB2022NSCQ-MSX0504), National Natural Science Foundation of China (No. 42305126), National Key Research and Development Program of China (No. 2023YFC3709301).

References

Akagi, S. K., Yokelson, R. J., Wiedinmyer, C., Alvarado, M. J., Reid, J. S., Karl, T., Crounse, J. D., and Wennberg, P. O.: Emission factors for open and domestic biomass burning for use in atmospheric models, Atmos. Chem. Phys., 11, 4039−4072, https://doi.org/10.5194/acp-11-4039-2011, 2011.

Alfarra, M. R., Prévôt, A. S. H., Szidat, S., Sandradewi, J., Sandradewi, S., Lanz, V. A., Schreiber, D., Mohr, M., and Baltensperger, U.: Identification of the Mass Spectral Signature of Organic Aerosols from Wood Burning Emissions, Environ. Sci. Technol., 41, 5770−5777, https://doi.org/10.1021/es062289b, 2007.

Bahreini, R., Ervens, B., Middlebrook, A. M., Warneke, C., de Gouw, J. A., DeCarlo, P. F., Jimenez, J. L., Brock, C. A., Neuman, J. A., Ryerson, T. B., Stark, H., Atlas, E., Brioude, J., Fried, A., Holloway, J. S., Peischl, J., Richter, D., Walega, J., Weibring, P., Wollny, A. G., and Fehsenfeld, F. C.: Organic Aerosol Formation in Urban and Industrial Plumes Near Houston and Dallas, Texas, J. Geophys. Res.: Atmos., 114, D00F16, doi:10.1029/2008JD011493, 2009.

Bao, Z. E., Liu, Y. L., Meng, L. S., Han, Y., Tian, M., Shi, G. M., Wang, Q. Y., Huang, Y., Peng, C., Luo, B., Zhang, W., Wang, H. B., Cao, J. J., Yang, F. M., and Chen, Y.: Evaluating the effects of biomass burning on severe haze formation in a megacity of Sichuan Basin, Southwestern China, J. Geophys. Res.: Atmos., 130, e2024JD042516, https://doi.org/10.1029/ 2024JD042516, 2025.

Bao, Z. E., Zeng, X. L., Zhou, J. W., Yang, F. M., Lu, K. D., Zhai, C. Z., Li, X., Feng, M., Tan, Q. W., and Chen, Y.: Evolution of black carbon and brown carbon during

718 summertime in Southwestern China: An assessment of control measures during the
719 2023 Chengdu Summer World University Games, Environ. Pollut., 357, 124467,
720 https://doi.org/10.1016/j.envpol.2024.124467, 2024.
721 Bao, Z. E., Zhang, X. Y., Li, Q., Zhou, J. W., Shi, G. M., Zhou, L., Yang, F. M., Xie, S.
722 D., Zhang, D., Zhai, C. Z., Li, Z. L., Peng, C., and Chen, Y.: Measurement report:
723 Intensive biomass burning emissions and rapid nitrate formation drive severe haze
724 formation in the Sichuan Basin, China – insights from aerosol mass spectrometry,
725 Atmos. Chem. Phys., 23, 1147−1167, https://doi.org/10.5194/acp-23-1147-2023,
726 2023.
727 Canagaratna, M. R., Jayne, J. T., Jimenez, J. L., Allan, J. D., Alfarra, M. R., Zhang, Q.,
728 Onasch, T. B., Drewnick, F., Coe, H., Middlebrook, A., Delia, A., Williams, L. R.,
729 Trimborn, A. M., Northway, M. J., DeCarlo, P. F., Kolb, C. E., Davidovits, P., and
730 Worsnop, D. R.: Chemical and microphysical characterization of ambient aerosols
731 with the aerodyne aerosol mass spectrometer, Mass Spectrom. Rev., 26, 185−222,
732 https://doi.org/10.1002/mas.20115, 2007.
733 Canagaratna, M. R., Jimenez, J. L., Kroll, J. H., Chen, Q., Kessler, S. H., Massoli, P.,
734 Hildebrandt Ruiz, L., Fortner, E., Williams, L. R., Wilson, K. R., Surratt, J. D.,
735 Donahue, N. M., Jayne, J. T., and Worsnop, D. R.: Elemental ratio measurements
736 of organic compounds using aerosol mass spectrometry: characterization,
737 improved calibration, and implications, Atmos. Chem. Phys., 15, 253−272,
738 https://doi.org/10.5194/acp-15-253-2015, 2015.
739 Canonaco, F., Crippa, M., Slowik, J. G., Baltensperger, U., and Prévôt, A. S. H.: SoFi,

an IGOR-based interface for the efficient use of the generalized multilinear engine (ME-2) for the source apportionment: ME-2 application to aerosol mass spectrometer data, Atmos. Meas. Tech., 6, 3649−3661, https://doi.org/10.5194/amt-6-3649-2013, 2013.

Carlton, A. G., Turpin, B. J., Altieri, K. E., Seitzinger, S., Reff, A., Lim, H. J., and Ervens, B.: Atmospheric oxalic acid and SOA production from glyoxal: results of aqueous photooxidation experiments, Atmos. Environ., 41, 7588−7602, https://doi.org/10.1016/j.atmosenv.2007.05.035, 2007.

Chen, C. R., Zhang, H. X., Yan, W. J., Wu, N. N., Zhang, Q., and He, K. B.: Aerosol water content enhancement leads to changes in the major formation mechanisms of nitrate and secondary organic aerosols in winter over the North China Plain, Environ. Pollut., 287, 117625, https://doi.org/10.1016/j.envpol.2021.117625, 2021.

Chen, Y., Tian, M., Huang, R. J., Shi, G. M., Wang, H. B., Peng, C., Cao, J. J., Wang, Q. Y., Zhang, S. M., Guo, D. M., Zhang, L. Y., and Yang, F. M.: Characterization of urban amine-containing particles in southwestern China: seasonal variation, source, and processing, Atmos. Chem. Phys., 19, 3245−3255, https://doi.org/10.5194/acp-19-3245-2019, 2019.

Chen, Y., Xie, S. D., Luo, B., and Zhai, C. Z.: Particulate pollution in urban Chongqing of southwest China: Historical trends of variation, chemical characteristics and source apportionment, Sci. Total Environ., 584−585, 523−534, https://doi.org/10.1016/j.scitotenv.2017.01.060, 2017.

Coen, M. C., Weingartner, E., Apituley, A., Ceburnis, D., Fierz-Schmidhauser, R.,

762 Flentje, H., Henzing, J. S., Jennings, S. G., Moerman, M., Petzold, A., Schmid, O.,
763 and Baltensperger, U.: Minimizing light absorption measurement artifacts of the
764 Aethalometer: Evaluation of five correction algorithms, Atmos. Meas. Tech., 3,
765 457−474, https://doi.org/10.5194/amt-3-457-2010, 2010.
766 Cubison, M. J., Ortega, A. M., Hayes, P. L., Farmer, D. K., Day, D., Lechner, M. J.,
767 Brune, W. H., Apel, E., Diskin, G. S., Fisher, J. A., Fuelberg, H. E., Hecobian, A.,
768 Knapp, D. J., Mikoviny, T., Riemer, D., Sachse, G. W., Sessions, W., Weber, R. J.,
769 Weinheimer, A. J., Wisthaler, A., and Jimenez, J. L.: Effects of aging on organic
770 aerosol from open biomass burning smoke in aircraft and laboratory studies, Atmos.
771 Chem. Phys., 11, 12049−12064, https://doi.org/10.5194/acp-11-12049-2011, 2011.
772 DeCarlo, P. F., Ulbrich, I. M., Crounse, J., de Foy, B., Dunlea, E. J., Aiken, A. C.,
773 Knapp, D., Weinheimer, A. J., Campos, T., Wennberg, P. O., and Jimenez, J. L.:
774 Investigation of the Sources and Processing of Organic Aerosol over the Central
775 Mexican Plateau from Aircraft Measurements during MILAGRO, Atmos. Chem.
776 Phys., 10, 5257−5280, https://doi.org/10.5194/acp-10-5257-2010, 2010.
777 Drinovec, L., Močnik, G., Zotter, P., Prévôt, A. S. H., Ruckstuhl, C., Coz, E.,
778 Rupakheti, M., Sciare, J., Müller, T., Wiedensohler, A., and Hansen, A. D. A.: The
779 "dual-spot" Aethalometer: an improved measurement of aerosol black carbon with
780 real-time loading compensation, Atmos. Meas. Tech., 8, 1965−1979,
781 https://doi.org/10.5194/amt-8-1965-2015, 2015.
782 Drozd, G. T. and McNeill, V. F.: Organic matrix effects on the formation of
783 light-absorbing compounds from α-dicarbonyls in aqueous salt solution, Environ.

Sci.: Processes Impacts, 16, 741−747, https://doi.org/10.1039/c3em00579h, 2014.

Elser, M., Huang, R. J., Wolf, R., Slowik, J. G., Wang, Q. Y., Canonaco, F., Li, G. H., Bozzetti, C., Daellenbach, K. R., Huang, Y., Zhang, R. J., Li, Z. Q., Cao, J. J., Baltensperger, U., El-Haddad, I., and Prévôt, A. S. H.: New insights into $PM_{2.5}$ chemical composition and sources in two major cities in China during extreme haze events using aerosol mass spectrometry, Atmos. Chem. Phys., 16, 3207−3225, https://doi.org/10.5194/acp-16-3207-2016, 2016.

Ervens, B., Turpin, B. J., and Weber, R. J.: Secondary organic aerosol formation in cloud droplets and aqueous particles (aqSOA): a review of laboratory, field and model studies, Atmos. Chem. Phys., 11, 11069−11102, https://doi.org/10.5194/acp-11-11069-2011, 2011.

Fountoukis, C. and Nenes, A.: ISORROPIA II: a computationally efficient thermodynamic equilibrium model for K^+–Ca^{2+}–Mg^{2+}–NH_4^+–Na^+–SO_4^{2-}–NO_3^-–Cl^-–H_2O aerosols, Atmos. Chem. Phys., 7, 4639−4659, https://doi.org/10.5194/acp-7-4639-2007, 2007.

Fröhlich, R., Cubison, M. J., Slowik, J. G., Bukowiecki, N., Prévôt, A. S. H., Baltensperger, U., Schneider, J., Kimmel, J. R., Gonin, M., Rohner, U., Worsnop, D. R., and Jayne, J. T.: The ToF-ACSM: a portable aerosol chemical speciation monitor with TOFMS detection, Atmos. Meas. Tech., 6, 3225−3241, https://doi.org/10.5194/amt-6-3225-2013, 2013.

Gilardoni, S., Massoli, P., Paglione, M., Giulianelli, L., Carbone, C., Rinaldi, M., Decesari, S., Sandrini, S., Costabile, F., Gobbi, G. P., Pietrogrande, M. C., Visentin,

M., Scotto, F., Fuzzi, S., and Facchini, M. C.: Direct observation of aqueous secondary organic aerosol from biomass-burning emissions, Proc. Natl. Acad. Sci. USA, 113, 10013−10018, https://doi.org/10.1073/pnas.1602212113, 2016.

Guo, H. Y., Xu, L., Bougiatioti, A., Cerully, K. M., Capps, S. L., Hite Jr., J.R., Carlton, A. G., Lee, S. H., Bergin, M. H., Ng, N. L., Nenes, A., and Weber, R. J.: Fine-particle water and pH in the southeastern United States, Atmos. Chem. Phys., 15, 5211−5228, https://doi.org/10.5194/acp-15-5211-2015, 2015.

Hennigan, C. J., Izumi, J., Sullivan, A. P., Weber, R. J., and Nenes, A.: A critical evaluation of proxy methods used to estimate the acidity of atmospheric particles, Atmos. Chem. Phys., 15, 2775–2790, https://doi.org/10.5194/acp-15-2775-2015, 2015.

Herrmann, H., Schaefer, T., Tilgner, A., Styler, S. A., Weller, C., Teich, M., and Otto, T.: Tropospheric Aqueous-Phase Chemistry: Kinetics, Mechanisms, and Its Coupling to a Changing Gas Phase, Chem. Rev., 115, 4259−4334, https://doi.org/10.1021/cr500447k, 2015.

Huang, R. J., Zhang, Y. L., Bozzetti, C., Ho, K. F., Cao, J. J., Han, Y. M., Daellenbach, K. R., Slowik, J. G., Platt, S. M., Canonaco, F., Zotter, P., Wolf, R., Pieber, S. M., Bruns, E. A., Crippa, M., Ciarelli, G., Piazzalunga, A., Schwikowski, M., Abbaszade, G., Schnelle-Kreis, J., Zimmermann, R., An, Z. S., Szidat, S., Baltensperger, U., El Haddad, I., and Prevot, A. S.: High secondary aerosol contribution to particulate pollution during haze events in China, Nature, 514, 218−222, https://doi.org/10.1038/nature13774, 2014.

828 Huang, R. J., He, Y., Duan, J., Li, Y. J., Chen, Q., Zheng, Y., Chen, Y., Hu, W. W., Lin,
829 C. S., Ni, H. Y., Dai, W. T., Cao, J. J., Wu, Y. F., Zhang, R. J., Xu, W., Ovadnevaite,
830 J., Ceburnis, D., Hoffmann, T., and O'Dowd, C. D.: Contrasting sources and
831 processes of particulate species in haze days with low and high relative humidity in
832 wintertime Beijing, Atmos. Chem. Phys., 20, 9101–9114,
833 https://doi.org/10.5194/acp-20-9101-2020, 2020.
834 Huang, X. J., Liu, Z., Ge, Y. Z., Li, Q., Wang, X. F., Fu, H. B., Zhu, J., Zhou, B.,
835 Wang, L., George, C., Wang, Y., Wang, X. F., Su, J. X., Xue, L. K., Yu, S. C.,
836 Mellouki, A., and Chen, J. M.: Aerosol high water contents favor sulfate and
837 secondary organic aerosol formation from fossil fuel combustion emissions, npj
838 Clim. Atmos. Sci., 6, 173, https://doi.org/10.1038/s41612-023-00504-1, 2023.
839 Jimenez, J. L., Canagaratna, M. R., Donahue, N. M., Prevot, A. S. H., Zhang, Q.,
840 Kroll, J. H., DeCarlo, P. F., Allan, J. D., Coe, H., Ng, N. L., Aiken, A. C., Docherty,
841 K. S., Ulbrich, I. M., Grieshop, A. P., Robinson, A. L., Duplissy, J., Smith, J. D.,
842 Wilson, K. R., Lanz, V. A., Hueglin, C., Sun, Y. L., Tian, J., Laaksonen, A.,
843 Raatikainen, T., Rautiainen, J., Vaattovaara, P., Ehn, M., Kulmala, M., Tomlinson, J.
844 M., Collins, D. R., Cubison, M. J., Dunlea, J., Huffman, J. A., Onasch, T. B.,
845 Alfarra, M. R., Williams, P. I., Bower, K., Kondo, Y., Schneider, J., Drewnick, F.,
846 Borrmann, S., Weimer, S., Demerjian, K., Salcedo, D., Cottrell, L., Griffin, R.,
847 Takami, A., Miyoshi, T., Hatakeyama, S., Shimono, A., Sun, J. Y., Zhang, Y. M.,
848 Dzepina, K., Kimmel, J. R., Sueper, D., Jayne, J. T., Herndon, S. C., Trimborn, A.
849 M., Williams, L. R., Wood, E. C., Middlebrook, A. M., Kolb, C. E., Baltensperger,

U., and Worsnop, D. R.: Evolution of Organic Aerosols in the Atmosphere, Science, 326, 1525−1529, https://doi.org/10.1126/science.1180353, 2009.

Kampf, C. J., Jakob, R., and Hoffmann, T.: Identification and characterization of aging products in the glyoxal/ammonium sulfate system – implications for light-absorbing material in atmospheric aerosols, Atmos. Chem. Phys., 12, 6323−6333, https://doi.org/10.5194/acp-12-6323-2012, 2012.

Kim, H., Collier, S., Ge, X. L., Xu, J. Z., Sun, Y. L., Jiang, W. Q., Wang, Y. L., Herckes, P., and Zhang, Q.: Chemical processing of water-soluble species and formation of secondary organic aerosol in fogs, Atmos. Environ., 200, 158−166, https://doi.org/10.1016/j.atmosenv.2018.11.062, 2019.

Kirchstetter, T. W. and Novakov T.: Evidence that the spectral dependence of light absorption by aerosols is affected by organic carbon, J. Geophys. Res., 109, D21208, https://doi.org/10.1029/2004JD004999, 2004.

Kondo, Y., Komazaki, Y., Miyazaki, Y., Moteki, N., Takegawa, N., Kodama, D., Deguchi, S., Nogami, M., Fukuda, M., Miyakawa, T., Morino, Y., Koike, M., Sakurai, H., and Ehara, K.: Temporal Variations of Elemental Carbon in Tokyo, J. Geophys. Res., 111, D12205, https://doi.org/10.1029/2005JD006257, 2006.

Kourtchev, I., Giorio, C., Manninen, A., Wilson, E., Mahon, B., Aalto, J., Kajos, M., Venables, D., Ruuskanen, T., Levula, J., Loponen, M., Connors, S., Harris, N., Zhao, D. F., Kiendler-Scharr, A., Mentel, T., Rudich, Y., Hallquist, M., Doussin, J. F., Maenhaut, W., Bäck, J., Petäjä, T., Wenger, J., Kulmala, Ma., and Kalberer, M.: Enhanced Volatile Organic Compounds emissions and organic aerosol mass

872 increase the oligomer content of atmospheric aerosols, Sci. Rep., 6, 35038,
873 https://doi.org/10.1038/srep35038, 2016.
874 Kroflic, A., Grilc, M., and Grgic, I.: Unraveling pathways of guaiacol nitration in
875 atmospheric waters: nitrite, a source of reactive nitronium ion in the atmosphere,
876 Environ. Sci. Technol., 49, 9150–9158, https://doi.org/10.1021/acs.est.5b01811,
877 2015.
878 Lanz, V. A., Alfarra, M. R., Baltensperger, U., Buchmann, B., Hueglin, C., and Prévôt,
879 A. S. H.: Source apportionment of submicron organic aerosols at an urban site by
880 factor analytical modelling of aerosol mass spectra, Atmos. Chem. Phys., 7,
881 1503–1522, doi:10.5194/acp-7-1503-2007, 2007.
882 Laskin, A., Laskin, J., and Nizkorodov, S. A.: Chemistry of atmospheric brown carbon,
883 Chem. Rev., 115, 4335−4382, https://doi.org/10.1021/cr5006167, 2015.
884 Lee, A. K., Zhao, R., Li, R., Liggio, J., Li, S. M., and Abbatt, J. P.: Formation of Light
885 Absorbing Organo-Nitrogen Species from Evaporation of Droplets Containing
886 Glyoxal and Ammonium Sulfate, Environ. Sci. Technol., 47, 12819−12826,
887 https://doi.org/10.1021/es402687w, 2013.
888 Lei, Y., Lei, X., Tian, G., Yang, J., Huang, D., Yang, X., Chen, C. C., and Zhao, J. C.:
889 Optical Variation and Molecular Transformation of Brown Carbon During
890 Oxidation by NO_3• in the Aqueous Phase, Environ. Sci. Technol., 58, 3353−3362,
891 https://doi.org/10.1021/acs.est.3c08726, 2024.
892 Li, C. L., He, Q. F., Fang, Z., Brown, S. S., Laskin, A., Cohen, S. R., and Rudich, Y.:
893 Laboratory Insights into the Diel Cycle of Optical and Chemical Transformations

of Biomass Burning Brown Carbon Aerosols, Environ. Sci. Technol., 54, 11827−11837, https://dx.doi.org/10.1021/acs.est.0c04310, 2020.

Li, F. H., Zhou, S. Z., Du, L., Zhao, J., Hang, J., and Wang, X. M.: Aqueous-phase chemistry of atmospheric phenolic compounds: A critical review of laboratory studies, Sci. Total Environ., 856, 158895, https://doi.org/10.1016/j.scitotenv.2022.158895, 2023.

Li, G., Bei, N., Tie, X., and Molina, L. T.: Aerosol effects on the photochemistry in Mexico City during MCMA-2006/MILAGRO campaign, Atmos. Chem. Phys., 11, 5169−5182, https://doi.org/10.5194/acp-11-5169-2011, 2011.

Lim, Y. B., Tan, Y., Perri, M. J., Seitzinger, S. P., and Turpin, B. J.: Aqueous chemistry and its role in secondary organic aerosol (SOA) formation, Atmos. Chem. Phys., 10, 10521−10539, https://doi.org/10.5194/acp-10-10521-2010, 2010.

Liu, M. X., Song, Y., Zhou, T., Xu, Z. Y., Yan, C. Q., Zheng, M., Wu, Z. J., Hu, M., Wu, Y. S., and Zhu, T.: Fine particle pH during severe haze episodes in northern China, Geophys. Res. Lett., 44, 5213−5221, https://doi.org/10.1002/2017gl073210, 2017.

Lorenzo, R. A. D., Washenfelder, R. A., Attwood, A. R., Guo, H., Xu, L., Ng, N. L., Weber, R. J., Baumann, K., Edgerton, E., and Young, C. J.: Molecular-Size-Separated Brown Carbon Absorption for Biomass-Burning Aerosol at Multiple Field Sites, Environ. Sci. Technol., 51, 3128−3137, https://doi.org/10.1021/acs.est.6b06160, 2017.

Lu, Z., Streets, D. G., Winijkul, E., Yan, F., Chen, Y., Bond, T. C., Feng, Y., Dubey, M.

K., Liu, S., Pinto, J. P., and Carmichael, G. R.: Light absorption properties and radiative effects of primary organic aerosol emissions, Environ. Sci. Technol., 49, 4868−4877, https://doi.org/10.1021/acs.est.5b00211, 2015.

Matthew, B. M., Middlebrook, A. M., and Onasch, T. B.: Collection Efficiencies in an Aerodyne Aerosol Mass Spectrometer as a Function of Particle Phase for Laboratory Generated Aerosols, Aerosol Sci. Technol., 42, 884−898, https://doi.org/10.1080/02786820802356797, 2008.

McNeill, V. F.: Aqueous Organic Chemistry in the Atmosphere: Sources and Chemical Processing of Organic Aerosols, Environ. Sci. Technol., 49, 1237−1244, https://doi.org/10.1021/es5043707, 2015.

Meng, J. J., Liu, X. D., Hou, Z. F., Yi, Y. A., Yan, L., Li, Z., Cao, J. J., Li, J. J., and Wang, G. H.: Molecular characteristics and stable carbon isotope compositions of dicarboxylic acids and related compounds in the urban atmosphere of the North China Plain: Implications for aqueous phase formation of SOA during the haze periods, Sci. Total Environ., 705, 135256, https://doi.org/10.1016/j.scitotenv.2019.135256, 2020.

Middlebrook, A. M., Bahreini, R., Jimenez, J. L., and Canagaratna, M. R.: Evaluation of Composition-Dependent Collection Efficiencies for the Aerodyne Aerosol Mass Spectrometer using Field Data, Aerosol Sci. Technol., 46, 258−271, https://doi.org/10.1080/02786826.2011.620041, 2012.

Ministry of Environmental Protection (MEP): P.R. Of China, China National Ambient Air Quality Standard (GB 3095-2012), http://kjs.mep.

gov.cn/hjbhbz/bzwb/dqhjbh/dqhjzlbz/201203/t20120302_224165.htm, 2012.

Moosmüller, H., Chakrabarty, R. K., and Arnott, W. P.: Aerosol light absorption and its measurement: A review, J. Quant. Spectrosc. Ra., 110, 844−878, https://doi.org/10.1016/j.jqsrt.2009.02.035, 2009.

Ng, N. L., Canagaratna, M. R., Jimenez, J. L., Chhabra, P. S., Seinfeld, J. H., and Worsnop, D. R.: Changes in organic aerosol composition with aging inferred from aerosol mass spectra, Atmos. Chem. Phys., 11, 6465−6474, https://doi.org/10.5194/acp-11-6465-2011, 2011a.

Ng, N. L., Canagaratna, M. R., Jimenez, J. L., Zhang, Q., Ulbrich, I. M., and Worsnop, D. R.: Real-Time Methods for Estimating Organic Component Mass Concentrations from Aerosol Mass Spectrometer Data, Environ. Sci. Technol., 45, 910−916, https://doi.org/10.1021/es102951k, 2011b.

Ng, N. L., Canagaratna, M. R., Zhang, Q., Jimenez, J. L., Tian, J., Ulbrich, I. M., Kroll, J. H., Docherty, K. S., Chhabra, P. S., Bahreini, R., Murphy, S. M., Seinfeld, J. H., Hildebrandt, L., Donahue, N. M., DeCarlo, P. F., Lanz, V. A., Prévôt, A. S. H., Dinar, E., Rudich, Y., and Worsnop, D. R.: Organic aerosol components observed in Northern Hemispheric datasets from Aerosol Mass Spectrometry, Atmos. Chem. Phys., 10, 4625−4641, https://doi.org/10.5194/acp-10-4625-2010, 2010.

Ng, N. L., Herndon, S. C., Trimborn, A., Canagaratna, M. R., Croteau, P. L., Onasch, T. B., Sueper, D., Worsnop, D. R., Zhang, Q., Sun, Y. L., and Jayne J. T.: An Aerosol Chemical Speciation Monitor (ACSM) for Routine Monitoring of the Composition and Mass Concentrations of Ambient Aerosol, Aerosol Sci. Technol.,

960 45, 780−794, https://doi.org/10.1080/02786826.2011.560211, 2011c.
961 Nguyen, T. K. V., Zhang, Q., Jimenez, J. L., Pike, M., and Carlton, A. G.: Liquid
962 Water: Ubiquitous Contributor to Aerosol Mass, Environ. Sci. Technol. Lett., 3,
963 257−263, https://doi.org/10.1021/acs.estlett.6b00167, 2016.
964 Nozière, B., and Esteve, W.: Light-absorbing aldol condensation products in acidic
965 aerosols: Spectra, kinetics, and contribution to the absorption index, Atmos.
966 Environ., 41, 1150−1163, https://doi.org/10.1016/j.atmosenv.2006.10.001, 2007.
967 Nozière, B., Dziedzic, P., and Córdova, A.: Products and Kinetics of the Liquid-Phase
968 Reaction of Glyoxal Catalyzed by Ammonium Ions (NH_4^+), J. Phys. Chem. A, 113,
969 231−237, https://doi.org/10.1021/jp8078293, 2009.
970 Ortega, A. M., Ortega, D. A., Cubison, M. J., Brune, W. H., Bon, D., Gouw de, J. A.,
971 and Jimenez, J. L.: Secondary organic aerosol formation and primary organic
972 aerosol oxidation from biomass-burning smoke in a flow reactor during FLAME-3,
973 Atmos. Chem. Phys., 13, 11551−11571,
974 https://doi.org/10.5194/acp-13-11551-2013, 2013.
975 Ortiz-Montalvo, D. L., Lim, Y. B., Perri, M. J., Seitzinger, S. P., and Turpin, B. J.:
976 Volatility and Yield of Glycolaldehyde SOA Formed through Aqueous
977 Photochemistry and Droplet Evaporation, Aerosol Sci. Technol., 46, 1002−1014,
978 https://doi.org/10.1080/02786826.2012.686676, 2012.
979 Paatero, P.: The Multilinear Engine: A Table-Driven, Least Squares Program for
980 Solving Multilinear Problems, Including the n-Way Parallel Factor Analysis Model,
981 J. Comput. Graph. Stat., 8, 854−888,

https://doi.org/10.1080/10618600.1999.10474853, 1999.

Paatero, P. and Hopke, P. K.: Discarding or downweighting high-noise variables in factor analytic models, Anal. Chim. Acta., 490, 277−289, https://doi.org/10.1016/S0003-2670(02)01643-4, 2003.

Paatero, P. and Tapper, U.: Positive matrix factorization: A non-negative factor model with optimal utilization of error estimates of data values, Environmetrics, 5, 111−126, https://doi.org/10.1002/env.3170050203, 1994.

Paglione, M., Gilardoni, S., Rinaldi, M., Decesari, S., Zanca, N., Sandrini, S., Giulianelli, L., Bacco, D., Ferrari, S., Poluzzi, V., Scotto, F., Trentini, A., Poulain, L., Herrmann, H., Wiedensohler, A., Canonaco, F., Prévôt, A. S. H., Massoli, P., Carbone, C., Facchini, M. C., and Fuzzi, S. C.: The impact of biomass burning and aqueous-phase processing on air quality: a multi-year source apportionment study in the Po Valley, Italy, Atmos. Chem. Phys., 20, 1233−1254, https://doi.org/10.5194/acp-20-1233-2020, 2020.

Pang, H. W., Zhang, Q., Lu, X. H., Li, K. N., Chen, H., Chen, J. M., Yang, X., Ma, Y. G., Ma, J. L., and Huang, C.: Nitrite-Mediated Photooxidation of Vanillin in the Atmospheric Aqueous Phase, Environ. Sci. Technol., 53, 14253−14263, https://doi.org/10.1021/acs.est.9b03649, 2019.

Peng, C., Tian, M., Shi, G. M., Zhang, S. M., Long, X., Che, H. X., Zhong, J., You, X. Y., Bao, Z. E., Yang, F. M., Qi, X., Zhai, C. Z., and Chen, Y.: Sources and light absorption of brown carbon in urban areas of the Sichuan Basin, China: Contribution from biomass burning and secondary formation, Atmos. Res., 318,

1004 107992, https://doi.org/10.1016/j.atmosres.2025.107992, 2025.
1005 Powelson, M. H., Espelien, B. M., Hawkins, L. N., Galloway, M. M., and Haan, D. O.
1006 D.: Brown Carbon Formation by Aqueous-Phase Carbonyl Compound Reactions
1007 with Amines and Ammonium Sulfate, Environ. Sci. Technol., 48, 985−993,
1008 https://doi.org/10.1021/es4038325, 2014.
1009 Qin, Y. M., Tan, H. B., Li, Y. J., Li, Z. J., Schurman, M. I., Liu, L., Wu, C., and Chan,
1010 C. K.: Chemical characteristics of brown carbon in atmospheric particles at a
1011 suburban site near Guangzhou, China, Atmos. Chem. Phys., 18, 16409−16418,
1012 https://doi.org/10.5194/acp-18-16409-2018, 2018.
1013 Saleh, R., Hennigan, C. J., McMeeking, G. R., Chuang, W. K., Robinson, E. S., Coe,
1014 H., Donahue, N. M., and Robinson, A. L.: Absorptivity of brown carbon in fresh
1015 and photo-chemically aged biomass-burning emissions, Atmos. Chem. Phys., 13,
1016 7683−7693, https://doi.org/10.5194/acp-13-7683-2013, 2013.
1017 Saleh, R., Robinson, E. S., Tkacik, D. S., Ahern, A. T., Liu, S., Aiken, A. C., Sullivan,
1018 R. C., Presto, A. A., Dubey, M. K., Yokelson, R. J., Donahue, N. M., and Robinson,
1019 A. L.: Brownness of organics in aerosols from biomass burning linked to their
1020 black carbon content, Nat. Geosci., 7, 647−650, https://doi.org/10.1038/ngeo2220,
1021 2014.
1022 Sareen, N., Moussa, S. G., and McNeill, V. F.: Photochemical Aging of
1023 Light-Absorbing Secondary Organic Aerosol Material, J. Phys. Chem. A, 117,
1024 2987−2996, https://doi.org/10.1021/jp309413j, 2013.
1025 Shrivastava, M., Cappa, C. D., Fan, J. W., Goldstein, A. H., Guenther, A. B., Jimenez,

J. L., Kuang, C. A., Laskin, A., Martin, S. T., Ng, N. L., Petaja, T., Pierce, J. R., Rasch, P. J., Roldin, P., Seinfeld, J. H., Shilling, J., Smith, J. N., Thornton, J. A., Volkamer, R., Wang, J., Worsnop, D. R., Zaveri, R. A., Zelenyuk, A., and Zhang, Q.: Recent advances in understanding secondary organic aerosol: Implications for global climate forcing, Rev. Geophys., 55, 509−559, doi:10.1002/2016RG000540, 2017.

Sun, Y. L., Du, W., Fu, P. Q., Wang, Q. Q., Li, J., Ge, X. L., Zhang, Q., Zhu, C. M., Ren, L. J., Xu, W. Q., Zhao, J., Han, T. T., Worsnop, D. R., and Wang, Z. F.: Primary and secondary aerosols in Beijing in winter: sources, variations and processes, Atmos. Chem. Phys., 16, 8309−8329, https://doi.org/10.5194/acp-16-8309-2016, 2016a.

Sun, Y. L., Jiang, Q., Xu, Y. S., Ma, Y., Zhang, Y. J., Liu, X. G., Li, W. J., Wang, F., Li, J., Wang, P. C., and Li, Z. Q.: Aerosol characterization over the North China Plain: Haze life cycle and biomass burning impacts in summer, J. Geophys. Res.: Atmos., 121, 2508−2521, https://doi.org/10.1002/ 2015jd024261, 2016b.

Sun, Y. L., Zhang, Q., Anastasio, C., and Sun, J.: Insights into secondary organic aerosol formed via aqueous-phase reactions of phenolic compounds based on high resolution mass spectrometry, Atmos. Chem. Phys., 10, 4809−4822, https://doi.org/10.5194/acp-10-4809-2010, 2010.

Tan, Y., Lim, Y. B., Altieri, K. E., Seitzinger, S. P., and Turpin, B. J.: Mechanisms leading to oligomers and SOA through aqueous photooxidation: insights from OH radical oxidation of acetic acid and methylglyoxal, Atmos. Chem. Phys., 12,

801−813, https://doi.org/10.5194/acp-12-801-2012, 2012.

Tao, J., Gao, J., Zhang, L., Zhang, R., Che, H., Zhang, Z., Lin, Z., Jing, J., Cao, J., and Hsu, S. C.: $PM_{2.5}$ pollution in a megacity of southwest China: source apportionment and implication, Atmos. Chem. Phys., c14, 8679−8699, https://doi.org/10.5194/acp-14-8679-2014, 2014.

Tian M., Liu Y., Yang F. M., Zhang L. M., Peng C., Chen Y., Shi G. M., Wang H. B., Luo B., Jiang C. T., Li B., Takeda N., and Koizumi K.: Increasing importance of nitrate formation for heavy aerosol pollution in two megacities in Sichuan Basin, southwest China, Environ. Pollut., 250, 898−905, https://doi.org/10.1016/j.envpol.2019.04.098, 2019.

Wang, G. H., Zhang, R. Y., Gomez, M. E., Yang, L. X., Zamora, M. L., Hu, M., Lin, Y., Peng, J. F., Guo, S., Meng, J. J., Li, J. J., Cheng, C. L., Hu T. F., Ren, Y. Q., Wang, Y. S., Gao, J., Cao, J. J., An, Z. S., Zhou, W. J., Li, G. H., Wang, J. Y., Tian, P. F., Marrero-Ortiz, W., Secrest, J., Du, Z. F., Zheng, J., Shang, D. J., Zeng, L. M., Shao, M., Wang, W. G., Huang, Y., Wang, Y., Zhu, Y. J., Li, Y. X., Hu, J. X., Pan, B., Cai, L., Cheng, Y. T., Ji, Y. M., Zhang, F., Rosenfeld, D., Liss, P. S., Duce, R. A., Kolb, C. E., and Molina, M. J.: Persistent sulfate formation from London Fog to Chinese haze, Proc. Natl. Acad. Sci. USA, 113, 13630−13635, https://doi.org/10.1073/pnas.1616540113, 2016.

Wang, H. B., Tian, M., Chen, Y., Shi, G. M., Liu, Y., Yang, F. M., Zhang, L. M., Deng, L. Q., Yu, J. Y., Peng, C., and Cao, X. Y.: Seasonal characteristics, formation mechanisms and source origins of $PM_{2.5}$ in two megacities in Sichuan Basin, China,

Atmos. Chem. Phys., 18, 865−881, https://doi.org/10.5194/acp-18-865-2018, 2018.

Wang, J. F., Ye, J. H., Zhang, Q., Zhao, J., Wu, Y. Z., Li, J. Y., Liu, D. T., Li, W. J., Zhang, Y. G., Wu, C., Xie, C. H., Qin, Y. M., Lei, Y. L., Huang, X. P., Guo, J. P., Liu, P. F., Fu, P. Q., Li, Y. J., Lee, H. C., Choi, H., Zhang, J., Liao, H., Chen, M. D., Sun, Y. L., Ge, X. L., Martin, S. T., and Jacob, D. J.: Aqueous production of secondary organic aerosol from fossil-fuel emissions in winter Beijing haze, Proc. Natl. Acad. Sci. USA, 118, e2022179118, https://doi.org/10.1073/pnas.2022179118, 2021.

Wang, Q. Y., Ye, J. H., Wang, Y. C., Zhang, T., Ran, W. K., Wu, Y. F., Tian, J., Li, L., Zhou, Y. Q., Ho, H. S. S., Dang, B., Zhang, Q., Zhang, R. J., Chen, Y., Zhu, C. S., and Cao, J. J.: Wintertime Optical Properties of Primary and Secondary Brown Carbon at a Regional Site in the North China Plain, Environ. Sci. Technol., 53, 12389−12397, https://doi.org/10.1021/acs.est.9b03406, 2019.

Washenfelder, R. A., Attwood, A. R., Brock, C. A., Guo, H., Xu, L., Weber, R. J., Ng, N. L., Allen, H. M., Ayres, B. R., Baumann, K., Cohen, R. C., Draper, D. C., Duffey, K. C., Edgerton, E., Fry, J. L., Hu, W. W., Jimenez, J. L., Palm, B. B., Romer, P., Stone, E. A., Wooldridge, P. J., and Brown, S. S.: Biomass burning dominates brown carbon absorption in the rural southeastern United States, Geophys. Res. Lett., 42, 653−664, https://doi.org/10.1002/2014gl062444, 2015.

Wu, C. and Yu, J. Z.: Determination of primary combustion source organic carbon-to-elemental carbon (OC/EC) ratio using ambient OC and EC measurements: Secondary OC-EC correlation minimization method, Atmos. Chem.

1092 Phys., 16, 5453−5465, https://doi.org/10.5194/acp-16-5453-2016, 2016.
1093 Wu, H., Peng, C., Zhai, T. Y., Deng, J. C., Lu, P. L., Li, Z. L., Chen, Y., Tian, M., Bao,
1094 Z. E., Long, X., Yang, F. M., and Zhai, C. Z.: Characteristics of light absorption
1095 and environmental effects of Brown carbon aerosol in Chongqing during summer
1096 and winter based on online measurement: Implications of secondary formation,
1097 Atmos. Environ., 338, 120843, https://doi.org/10.1016/j.atmosenv.2024.120843,
1098 2024.
1099 Xie, C. H., Xu, W. Q., Wang, J. F., Wang, Q. Q., Liu, D. T., Tang, G. Q., Chen, P., Du,
1100 W., Zhao, J., Zhang, Y. J., Zhou, W., Han, T. T., Bian, Q. Y., Li, J., Fu, P. Q., Wang,
1101 Z. F., Ge, X. L., Allan, J., Coe, H., and Sun, Y. L.: Vertical characterization of
1102 aerosol optical properties and brown carbon in winter in urban Beijing, China,
1103 Atmos. Chem. Phys., 19, 165−179, https://doi.org/10.5194/acp-19-165-2019, 2019.
1104 Xu, B. Q., Zhang, G., Gustafsson, Ö., Kawamura, K., Li, J., Andersson, A., Bikkina,
1105 S., Kunwar, B., Pokhrel, A., Zhong, G. C., Zhao, S. Z., Li, J., Huang, C., Cheng, Z.
1106 N., Zhu, S. Y., Peng, P. A., and Sheng, G. Y.: Large contribution of fossil-derived
1107 components to aqueous secondary organic aerosols in China, Nat. Commun., 13,
1108 5115, https://doi.org/10.1038/s41467-022-32863-3, 2022.
1109 Xu, W. Q., Han, T. T., Du, W., Wang, Q. Q., Chen, C., Zhao, J., Zhang, Y. J., Li, J., Fu,
1110 P. Q., Wang, Z. F., Worsnop, D. R., and Sun, Y. L.: Effects of Aqueous-Phase and
1111 Photochemical Processing on Secondary Organic Aerosol Formation and Evolution
1112 in Beijing, China, Environ. Sci. Technol., 51, 762−770,
1113 https://doi.org/10.1021/acs.est.6b04498, 2017.

Xu, W. Q., Sun, Y. L., Chen, C., Du, W., Han, T. T., Wang, Q. Q., Fu, P. Q., Wang, Z. F., Zhao, X. J., Zhou, L. B., Ji, D. S., Wang, P. C., and Worsnop, D. R.: Aerosol composition, oxidation properties, and sources in Beijing: results from the 2014 Asia-Pacific Economic Cooperation summit study, Atmos. Chem. Phys., 15, 13681−13698, https://doi.org/10.5194/acp-15-13681-2015, 2015.

Xu, W. Q., Sun, Y. L., Wang, Q. Q., Zhao, J., Wang, J. F., Ge, X. L., Xie, C. J., Zhou, W., Du, W., Li, J., Fu, P. Q., Wang, Z. F., Worsnop, D. R., and Coe, H.: Changes in Aerosol Chemistry From 2014 to 2016 in Winter in Beijing: Insights From High-Resolution Aerosol Mass Spectrometry, J. Geophys. Res.: Atmos., 124, 1132−1147, https://doi.org/10.1029/2018JD029245, 2019.

Yan, C. Q., Zheng, M., Bosch, C., Andersson, A., Desyaterik, Y., Sullivan, A. P., Collett, J. L., Zhao, B., Wang, S. X., He, K. B., and Gustafsson, Ö.: Important fossil source contribution to brown carbon in Beijing during winter, Sci. Rep., 7, 43182, https://doi.org/10.1038/srep43182, 2017.

Yang, J. W., Au, W. C., Law, H., Lam, C. H., and Nah, T.: Formation and evolution of brown carbon during aqueous-phase nitrate-mediated photooxidation of guaiacol and 5-nitroguaiacol, Atmos. Environ., 254, 118401, https://doi.org/10.1016/j.atmosenv.2021.118401, 2021.

Yang, F. M., Tan, J., Zhao, Q., Du, Z., He, K. B., Ma, Y. L., Duan, F. K., Chen, G., and Zhao, Q.: Characteristics of $PM_{2.5}$ speciation in representative megacities and across China, Atmos. Chem. Phys., 11, 5207−5219, https://doi.org/10.5194/acp-11-5207-2011, 2011.

Ye, Z. L., Qu, Z. X., Ma, S. S., Luo, S. P., Chen, Y. T., Chen, H., Chen, Y. F., Zhao, Z. Z., Chen, M. D., and Ge, X. L.: A comprehensive investigation of aqueous-phase photochemical oxidation of 4-ethylphenol, Sci. Total Environ., 685, 976−985, https://doi.org/10.1016/j.scitotenv.2019.06.276, 2019.

Yokelson, R. J., Urbanski, S. P., Atlas, E. L., Toohey, D. W., Alvarado, E. C., Crounse, J. D., Wennberg, P. O., Fisher, M. E., Wold, C. E., Campos, T. L., Adachi, K., Buseck, P. R., and Hao, W. M.: Emissions from forest fires near Mexico City, Atmos. Chem. Phys., 7, 5569−5584, https://doi.org/10.5194/acp-7-5569-2007, 2007.

Yu, L., Smith, J., Laskin, A., Anastasio, C., Laskin, J., Zhang, Q.: Chemical characterization of SOA formed from aqueous-phase reactions of phenols with the triplet excited state of carbonyl and hydroxyl radical, Atmos. Chem. Phys., 14, 13801−13816, https://doi.org/10.5194/acp-14-13801-2014, 2014.

Yu, L., Smith, J., Laskin, A., George, K. M., Anastasio, C., Laskin, J., Dillner, A. M., and Zhang, Q.: Molecular transformations of phenolic SOA during photochemical aging in the aqueous phase: competition among oligomerization, functionalization, and fragmentation, Atmos. Chem. Phys., 16, 4511−4527, https://doi.org/10.5194/acp-16-4511-2016, 2016.

Zhao, J., Du, W., Zhang, Y. J., Wang, Q. Q., Chen, C., Xu, W. Q., Han, T. T., Wang, Y. Y., Fu, P. Q., Wang, Z. F., Li, Z. Q., and Sun, Y. L.: Insights into aerosol chemistry during the 2015 China Victory Day parade: results from simultaneous measurements at ground level and 260 m in Beijing, Atmos. Chem. Phys., 17,

3215−3232, https://doi.org/10.5194/acp-17-3215-2017, 2017.

Zhao, J., Qiu, Y. M.,Zhou, W., Xu, W. Q., Wang, J. F., Zhang, Y. J., Li, L. J., Xie, C. H., Wang, Q. Q., Du, W., Worsnop, D. R., Canagaratna, M. R., Zhou, L. B., Ge, X. L., Fu, P. Q., Li, J., Wang, Z. F., Donahue, N. M., and Sun, Y. L.: Organic Aerosol Processing During Winter Severe Haze Episodes in Beijing, J. Geophys. Res.: Atmos., 124, 10248−10263, https://doi.org/10.1029/2019JD030832, 2019.

Zhao, R., Lee, A. K. Y., Huang, L., Li, X., Yang, F., and Abbatt, J. P. D.: Photochemical processing of aqueous atmospheric brown carbon, Atmos. Chem. Phys., 15, 6087−6100, https://doi.org/10.5194/acp-15-6087-2015, 2015.

Zhao, R., Mungall, E. L., Lee, A. K. Y., Aljawhary, D., and Abbatt, J. P. D.: Aqueous-phase photooxidation of levoglucosan – a mechanistic study using aerosol time-of-flight chemical ionization mass spectrometry (Aerosol ToF-CIMS), Atmos. Chem. Phys., 14, 9695−9706, https://doi.org/10.5194/acp-14-9695-2014, 2014.

Zhong, H. B., Huang, R. J., Chang, Y. H., Duan, J., Lin, C. S., and Chen, Y.: Enhanced formation of secondary organic aerosol from photochemical oxidation during the COVID-19 lockdown in a background site in Northwest China, Sci. Total Environ., 778, 144947, https://doi.org/10.1016/j.scitotenv.2021.144947, 2021.

Zhu, C. S., Cao, J. J., Hu, T. F., Shen, Z. X., Tie, X. X., Huang, H., Wang, Q. Y., Huang, R. J., Zhao, Z. Z., Mocnik, G., and Hansen, A. D. A.: Spectral dependence of aerosol light absorption at an urban and a remote site over the Tibetan Plateau,

1180 Sci. Total Environ., 590−591, 14−21,
1181 https://doi.org/10.1016/j.scitotenv.2017.03.057, 2017.